Major hydrological shifts in the Black Sea "Lake" in response to ice sheet collapses during MIS 6 (130-184 ka BP)

for publication in "*Quaternary Science Reviews*" by

Antje Wegwerth[a*], Olaf Dellwig[a], Sabine Wulf[b,c], Birgit Plessen[b], Ilka C. Kleinhanns[d], Norbert R. Nowaczyk[b], Liu Jiabo[b], and Helge W. Arz[a]

[a]Leibniz-Institute for Baltic Sea Research Warnemünde (IOW), Marine Geology, Rostock, Germany

[b]Helmholtz Centre Potsdam, GFZ German Research Centre for Geosciences, Section Climate Dynamics and Landscape evolution, Potsdam, Germany

[c]Department of Geography, University of Portsmouth, Portsmouth, United Kingdom

[d]Isotope Geochemistry, Department of Earth Sciences, University of Tübingen, Germany

Highlights

• Black Sea "Lake" record between 184 ka BP and 124 ka BP (MIS 6-5e) is presented.

• Main parameters are $\delta^{18}O$, $^{87}Sr/^{86}Sr$, Sr/Ca, and Mg/Ca of ostracods.

• Higher temperatures and stadial-interstadial variability during early MIS 6.

• Three long-term meltwater periods during insolation maxima and retreated ice sheets.

• Caspian–Black Sea connection during meltwater periods, but different sources/pathways.

* Corresponding author: Antje Wegwerth
e-mail/phone: antje.wegwerth@io-warnemuende.de / +49-381-5197-3481

Major hydrological shifts in the Black Sea "Lake" in response to ice sheet collapses during MIS 6 (130-184 ka BP)

for publication in "*Quaternary Science Reviews*" by

Antje Wegwerth[a*], Olaf Dellwig[a], Sabine Wulf[b,c], Birgit Plessen[b], Ilka C. Kleinhanns[d], Norbert R. Nowaczyk[b], Liu Jiabo[b], and Helge W. Arz[a]

[a]Leibniz Institute for Baltic Sea Research Warnemünde (IOW), Marine Geology, Rostock, Germany

[b]Helmholtz Centre Potsdam, GFZ German Research Centre for Geosciences, Section Climate Dynamics and Landscape evolution, Potsdam, Germany

[c]Department of Geography, University of Portsmouth, Portsmouth, United Kingdom

[d]Isotope Geochemistry, Department of Earth Sciences, University of Tübingen, Germany

[*] Corresponding author: Antje Wegwerth
e-mail/phone: antje.wegwerth@io-warnemuende.de / +49-381-5197-3481

Abstract

The Saalian was one of the largest glaciations during the Quaternary with an ice sheet extending considerably wider into the Eurasian continent than during other glacials. Orbital variations caused the ice sheet to switch between growing and shrinking. The partial retreat of the ice sheet and meltwater discharge resulted in global sea-level rise and increased lake levels of inland seas with broader environmental implications. During Marine Isotope Stage 6 (MIS 6), meltwater entered the formerly enclosed Black Sea at least twice as documented in a $\delta^{18}O$ record from Anatolian speleothems. Here we present a sedimentary record from the Black Sea "Lake" covering MIS 6 and provide evidence for three meltwater periods coinciding with insolation maxima (BSWP-6-1: 180-167 ka BP, BSWP-6-2: 160-145 ka BP, BSWP-II: 133-130 ka BP). While $\delta^{18}O_{ostracods}$ and $Sr/Ca_{ostracods}$ point to pronounced meltwater supply and decreasing salinity, $^{87}Sr/^{86}Sr_{ostracods}$ shed light on meltwater sources and pathways. During all three periods, meltwater drained most likely via the Dnieper and Volga into the Black and Caspian Seas and connected both basins. Relatively low $^{87}Sr/^{86}Sr_{ostracods}$ values during the oldest meltwater period suggest melting solely of the eastern Eurasian Ice Sheet. In contrast, during the younger meltwater periods, exceptional high $^{87}Sr/^{86}Sr_{ostracods}$ values point towards additional meltwater from the western Eurasian Ice Sheet. A surplus from melting glaciers in the Tian Shan and Pamir Mountains that finally entered the Caspian Sea via the Amu Darya and Sry Darya probably amplified the input of high radiogenic Sr-isotope water. We also show that higher temperatures and productivity suggest Dansgaard-Oeschger-like climate variability during the first half of MIS 6.

Keywords

MIS 6, Black Sea "Lake", meltwater, $\delta^{18}O_{ostracods}$, $^{87}Sr/^{86}Sr_{ostracods}$, tephra, palaeohydrology, Pleistocene, Saalian Glaciation, Eurasia, Radiogenic isotopes

1. Introduction

Earth's climate is very sensitive and fluctuates on various timescales triggered by the interaction between external forcing (e.g. insolation) and internal feedback (e.g. ice sheet volume, albedo, greenhouse gases, atmospheric/oceanic circulation; Milanković, 1969; Imbrie et al., 1989; Abe-Ouchi et al., 2013). Due to minimum insolation on Earth, continental ice sheets covered large parts of the northern hemisphere during the last two glacials, the Saalian and Weichselian, causing global sea level fall (Berger and Loutre, 1991; Svendsen et al., 2004; Bintanja and van de Wal., 2008). The disintegration of the continental ice sheets during glacial-interglacial transitions (terminations) and within milder periods during the glacials resulted in a rising global sea level (Bintanja and van de Wal, 2008; Grant et al., 2012, 2014). The Saalian Eurasian Ice Sheet extended considerably wider south-eastward into the continent and its most southern component, the Dnieper lobe stretched as far as 50°N (Svendsen et al., 2004; Ehlers and Gibbard, 2007; Colleoni et al., 2016; Hughes and Gibbard, 2018; Marks et al., 2018). In contrast, the last glacial Eurasian Ice Sheet margin covered an area between ca. 55°N and 60°N and was much less in touch with the Eurasian landmasses (Svendsen et al., 2004). The maximum ice thickness during the Saalian was 4,500 m with its centre located over the Kara Sea (Lambeck et al., 2006), whereas during the Weichselian it was 3,000 m high and centred over the Barents Sea (Lambeck, 1996). The much larger ice sheet extent during the Saalian likely resulted in colder inland climate conditions. The history of the waxing and waning Eurasian Ice Sheet with estimation of its extent across the continent is best documented for the last glacial (e.g., Svendsen et al., 2004; Lambeck et al., 2006; Larsen et al., 2006; Hughes et al., 2016), whereas reconstructions of the Saalian Ice Sheet are mainly limited to the penultimate glacial maximum around 140 ka BP (Svendsen et al., 2004).

Another feature of the glacial climate system is a pronounced millennial- to centennial-scale climate variability (i.e. during Marine Isotope Stages (MIS) 2-4; 14-71 ka BP) expressed by severe worldwide oscillations in temperature, rainfall, and wind intensity (e.g. Heinrich,

1988; Dansgaard et al., 1993; Sima et al., 2013). The so-called Dansgaard-Oeschger (DO) cycles were originally detected by $\delta^{18}O$ variations in Greenland ice cores (Dansgaard et al., 1993) showing alternations between abrupt warming during interstadials and gradual cooling during stadials. Previous studies have shown that the Black Sea sediments deposited during the last glacial document these DO cycles exceptionally well (Nowaczyk et al., 2012; Shumilovskikh et al., 2014; Wegwerth et al., 2015, 2016). Similar climate variations may have also occurred during the penultimate glacial as suggested from a synthetic Greenland ice core record (Barker et al., 2011).

Proxy-based evidence for climate changes, on both glacial-interglacial and millennial timescales, is provided from sediment and ice cores as well as from speleothems worldwide (e.g., Dansgaard et al., 1993; Martrat et al., 2004; Wang et al., 2008). Nevertheless, continental archives from the Eurasian interior recording climate change during the last ~200 kyrs are comparatively rare although these could highly contribute to our understanding of the atmospheric circulation patterns in a hemisphere-wide perspective. In addition to speleothems, loess, and lacustrine sediment cores from e.g. lakes Van, Urmia, and Ohrid (e.g., Fleitmann et al., 2009; Vogel et al., 2010; Stevens et al., 2012; Çağatay et al., 2014; Francke et al., 2016; Stockhecke et al., 2016; Sinopoli et al., 2018), glacial deposits from the Black Sea, bridging the Atlantic-Eurasian corridor, represent an ideal continental archive for global and regional palaeoclimate and environmental change.

Compared to Termination I (T I), much less is known about the penultimate glacial-interglacial transition (Termination II (T II); MIS 6/5) due to the lack of suitable sediment cores from the Black Sea. A ~56% larger Fennoscandian Ice Sheet expanding further east and southeast during MIS 6, compared to the last glacial (Svendsen et al., 2004; Colleoni et al., 2009; Marks et al., 2018), potentially caused an even stronger impact on major atmospheric circulation patterns and climate conditions in this region. Therefore, it is of particular interest

to understand how the Black Sea responded to the changing climate during the penultimate glacial (MIS 6; Saalian) and T II.

A well-dated $\delta^{18}O$ record from Northern Anatolian speleothems documents several hydrological shifts in the Black Sea region during the last 670 kyrs (Badertscher et al., 2011). Pronounced negative excursions in this record indicate that high amounts of freshwater entered the Black Sea in response to melting of the Eurasian Ice Sheet. The most depleted $\delta^{18}O$ values in that discontinuous record were assumed to reflect connections between the Caspian and Black Seas at least during seven intervals. Thus, apart from the Dnieper, meltwater fed the Volga River that resulted in lake-level rise of the Caspian Sea and overflow of isotopically lighter Caspian water into the Black Sea via the Manych Depression (Chepalyga, 2007; Bahr et al., 2008). The negative excursions in the $\delta^{18}O$ records of ostracods from the Black Sea support a Caspian-Black Sea connection at least during the deglaciations during the last two terminations (Bahr et al., 2008; Shumilovskikh et al., 2013b; Wegwerth et al., 2014). However, due to the lack of appropriate sediment cores covering older periods, the other suggested Caspian connections could not be tested by $\delta^{18}O$ signatures on Black Sea ostracods so far.

Because of relatively high sedimentation rates in the highly studied western and northwestern parts of the Black Sea basin, sediments covering the penultimate glacial are only found in sub-bottom depths larger than 100 m (Quan et al., 2013), thus ruling out recovery by conventional coring (e.g. gravity/piston corer). During RV Meteor cruise M72/5 in 2007 well-preserved sediment cores covering the ending penultimate glacial and the Eemian were obtained from the SE Black Sea because of up to 10 times lower sedimentation rates there (e.g., Shumilovskikh et al., 2013a, 2013b, Wegwerth et al., 2014). Detailed investigations on these sediment cores provided new findings about the environmental and climate conditions during T II (Shumilovskikh et al., 2013a, 2013b, Wegwerth et al., 2014, 2018; Dellwig et al., 2019). In response to the disintegrating Fennoscandian Ice Sheet, two discrete meltwater pulses resulted in pronounced freshwater supply during the late penultimate glacial at 133.5–132.5 ka

BP (BSWP-II-1) and 131.5–130.5 ka BP (BSWP-II-2) (Shumilovskikh et al., 2013a, 2013b; Wegwerth et al., 2014). This period of meltwater release coincides with ice-sheet simulations for the northern hemisphere showing a significant retreat of the ice sheet at 132 ka BP (Menviel et al., 2018). Higher radiogenic $^{87}Sr/^{86}Sr_{ostracods}$ values for the second T II meltwater pulse even suggest a freshwater surplus from a Himalayan source (Wegwerth et al., 2014), not observed for the T I meltwater pulse (Major et al., 2006). Warming during T II was gradual without a Younger Dryas-type cooling, although often postulated at least for the North Atlantic realm (Sarnthein and Tiedemann, 1990; Lototskaya and Ganssen, 1999). Although essential for the understanding of the climate mechanisms under different boundary conditions (e.g. insolation, ice sheet size, sea level), the climate and environmental Black Sea evolution during the penultimate glacial older than 134 ka BP is still unknown.

During RV Maria S. Merian cruise MSM 33 in 2013, the Archangelsky Ridge in the SE Black Sea was revisited in order to extend the sedimentary records to MIS 6 and even further to investigate the climate and environmental conditions in response to the dynamics of the Saalian Eurasian Ice Sheet (Arz et al., 2014). The new sediment cores extend to at least 184 ka BP and, thus, allow for the first time the investigation of almost the entire MIS 6. This opens the opportunity to contribute to the understanding of the environmental conditions in the Eurasian continental interior since terrestrial records, particularly those far from the ocean, comprising the MIS 6 are missing (Wainer et al., 2013; Margari et al., 2014). Obrochta et al. (2014) proposed a substantially differing penultimate glacial when compared with the preceding and subsequent glacials probably due to different boundary conditions including insolation and ice sheet expansion. Alike the last glacial, millennial-scale DO-like climate variability prevailed during MIS 6 at least until 155 ka BP as suggested from North Atlantic sediment cores (Margari et al., 2014). Cold events during MIS 6 probably lasted longer compared to the last glacial (MIS 2-4), which is explained by the background climate state

resulting in a reduced ocean heat transport associated with a smaller threshold for disruption of the Atlantic Meridional overturning circulation (Margari et al., 2010).

2. Climate and environmental setting of the Black Sea region

Today, the climate in the Black Sea region is governed by Mediterranean cyclones, the continental Siberian High Pressure system as well as the Indian and East African monsoons causing dry/warm summers and wet/cold winters (e.g., Wigley and Farmer, 1982; Cullen and deMenocal, 2000; Lamy et al., 2006; Göktürk et al., 2011). Therefore, Black Sea sediments represent appropriate recorders of changes in the interaction of the ocean-atmosphere-land system over Eurasia. The most rain-laden regions during summer are northeastern Anatolia and the eastern Black Sea due to orographic precipitation in the Pontic and Caucasian Mountains (Staneva and Stanev, 1998; Türkes et al., 2009; Deniz et al., 2011). An additional moisture source for rainfall forms the Black Sea itself (Fleitmann et al., 2009; Badertscher et al., 2011; Göktürk et al., 2011).

The main rivers entering the Black Sea are Danube, Dniester, Dnieper, and Don in the northwest and Yesilirmak, Kizilirmak, and Sakarya in the south (Fig. 1), with the river Danube contributing about 50%-70% of the total freshwater input (Özsoy and Ünlüata, 1997; Nezlin, 2006). Today, the Black Sea receives high salinity water (35.5‰) from the Mediterranean Sea via the Dardanelles and Bosporus straits. The Black Sea salinity ranges from about 18‰ in surface water to 22.4‰ in the bottom waters (Özsoy and Ünlüata, 1997). A permanent pycnocline in about 100-150m water depth prevents vertical exchange of water masses and deep-water ventilation. A pelagic redoxcline in this depth interval separates oxic surface water from sulphidic water favouring sapropel formation (Murray, 1900; Repeta et al., 1989; Özsoy and Ünlüata, 1997; Murray et al., 2007; Dellwig et al., 2010). With a maximum depth of about 2200m, the Black Sea represents the largest brackish and sulphidic water body on Earth (Demaison and Moore, 1980; Özsoy and Ünlüata, 1997).

3. Material and methods

This study is based on the analysis of three sediment cores recovered from the Archangelsky Ridge in the SE Black Sea during RV Maria S. Merian cruise MSM33 in 2013 (Fig. 1). The gravity cores (MSM33/60-1GC, MSM33/57-1GC, and MSM33/56-1GC) were retrieved from water depths between 374 m and 499 m and are mainly composed of glacial clays. Apart from the Holocene sapropel at the top of the cores, core MSM33/60-1GC additionally includes the Eemian sapropel between the limnic sediments from the Weichselian and Saalian glacials. In this study, we focus on sediments older than the Eemian and combine the three cores for a composite record covering Marine isotope Stage 6 of the penultimate glacial. In addition to ostracod and inorganic sediment geochemistry, three distinct tephra marker horizons from MSM33/60-1GC and three additional tephra samples from parallel cores MSM33/61-1GC and M72/5/22GC-8 were analysed with regards to their geochemical composition for independent chronostratigraphic control. Generally, the analyses were carried out on a 1 cm resolution. Unless noted otherwise, analyses were made at the Leibniz Institute for Baltic Sea Research Warnemünde, Rostock, Germany.

3.1 Electron probe microanalyses (EPMA) of tephra layers

For the element composition of macroscopically visible tephra layers, glass shards were identified, hand-picked under a transmitted microscope, and resin-embedded into single-hole stubs from the dried and wet-sieved sediment fraction 63-150 µm in cores MSM33/60-1GC, MSM33/61-1 GC and M72/5/22GC-8. The major element composition of single glass shards was analysed at the German Research Centre for Geosciences GFZ in Potsdam, Germany, using a JEOL JXA-8230 (WDS) microprobe with five spectrometers. Analytical setups used 15 kV accelerating voltage, 10 nA beam current, and a 5-10 µm beam. Count times per element were 20 seconds for Fe, Mn, Ti, Mg, P and Cl, and 10 seconds for Si, Al, K, Ca, F and Na measured first. Prior to sample analyses, common mineral standards, MPI glass standards (ATHO-G,

StHs6/80 and GOR-132; Jochum et al., 2006) and the natural Lipari obsidian (Hunt and Hill, 1996; Kuehn et al., 2011) were measured for instrumental calibration and data quality verification. All tephra sample data were normalized to 100 wt% on a volatile-free basis and plotted in bivariate elemental diagrams for interpretation. The raw EPMA dataset can be found in the supplementary material.

3.2 Ostracod geochemistry and IRD_C

For geochemical analyses of the ostracods, well-preserved valves of adult specimens of *Candona* spp. and *Bacuniella dorsoarcuata* (Zalanyi, 1929 in Boomer, 2012) were hand-picked from the wet-sieved and dried sediment fraction >150 µm.

For Mg/Ca and Sr/Ca ratios of the carbonate shells, the valves were cleaned with a thin brush and deionised water. After dissolution of up to five valves in 2 vol% HNO_3 (sub-boiled), the ostracod´s element/Ca ratios were determined by quadrupol ICP-MS (iCAP Q; Thermo Fisher Scientific) in KED mode using He as collision gas. For compensation of matrix effects and instrument fluctuations, Be and Rh were added to each solution as internal standards. Al was measured for monitoring potential detrital contamination. Analyses of total digestion of the international reference material ECRM 752-1 (BCS-CRM No 393; n=87) assured a precision and trueness of <0.9% and < 3.3% for Mg, <1.5% and <0.6% for Sr, and <1.1% and -1.9% for Ca, respectively.

For the oxygen isotopic composition of the ostracods, the pre-cleaned valves (20-80 µg) were measured with a Finnigan MAT 253 isotope ratio mass spectrometer coupled with an automated KIEL IV carbonate preparation device (103% H_3PO_4 at 70°C) at the GFZ Potsdam, Germany. Oxygen isotope values are given in delta notation relative to VPDB (Vienna Peedee Belemnite). Repeated measurements of the international reference material NBS 19 and a laboratory internal standard (C1) assured an analytical precision better than ±0.07‰ for $\delta^{18}O_{ostracods}$. Because several samples (n=70) contained none or only few ostracods of *Candona*

241 spp., *Bacuniella dorsoarcuata* was analysed for $\delta^{18}O$ in these samples. To correct for potential
242 species-dependent offsets, nine samples containing both species were analysed for $\delta^{18}O_{ostracods}$.
243 The positive correlation (R^2 = 0.99; y = 0.45318 + 0.93333x) between $\delta^{18}O_{Candona}$ and
244 $\delta^{18}O_{Bacuniella}$ was used to correct $\delta^{18}O_{Bacuniella}$ relative to $\delta^{18}O_{Candona}$ by an offset of +0.45‰.
245 For the analyses of the strontium isotopic composition, 10-15 ostracod valves were
246 cleaned with a few drops of H_2O_2 (5%), methanol, and deionised water (Janz and Vennemann,
247 2005; Major et al., 2006; Vasiliev et al., 2010). After dissolution of the valves in 300µL 2 vol%
248 HNO_3, the samples were dried on a hot plate at 80°C. Strontium was separated from the sample
249 matrix by using the HNO_3–H_2O technique in microcolumns filled with Eichrom© Sr-spec resin.
250 Dried Sr separates were re-dissolved in 0.3 N HNO_3. In static mode, fully automated isotope
251 ratio measurements were performed with a MC-ICP-MS (Neptune Plus, Thermo) at the
252 University of Tübingen, Germany. Instrumental mass bias was corrected using an $^{88}Sr/^{86}Sr$ ratio
253 of 8.375209 and exponential law. External reproducibility for NBS SRM 987 (n =30) was
254 0.710261 ± 0.000019 (2 s.d.) for the $^{87}Sr/^{86}Sr$ ratio and the total procedural blank was <306 pg
255 for Sr.
256 The amount of coastal ice-rafted detritus (IRD_C) was determined by counting the detrital
257 grains from 8.8 cm^3 subsamples of the dried and wet-sieved sediment fraction >150 µm under
258 a binocular microscope (Nowaczyk et al., 2012).
259
260 **3.3 Sediment geochemistry**
261 Except for X-ray fluorescence (XRF) core scanning, all other geochemical analyses were
262 carried out on freeze-dried and homogenised sediment sample aliquots.
263
264 *3.3.1 Bulk parameter*
265 The amount of total carbon (TC) was measured after combustion by an elemental analyser
266 EA 1110 (CE-instruments). The content of total organic carbon (TOC) was determined on in-

situ decalcified samples. Between 0.5 and 5 mg of bulk sample material was treated with 20% HCl in Ag-capsules, dried at 75°C, finally wrapped and measured by an elemental analyser Carlo-Erba NC2500 at GFZ Potsdam, Germany. The calibration was performed using elemental standard (Urea) and proofed with a soil reference sample (Boden3, HEKATECH) with a reproducibility for replicate analyses of 0.2%. Total inorganic carbon (TIC) was calculated by the difference between TC and TOC.

3.3.2. Inorganic sediment geochemistry

High-resolution core scanning (1 mm) of Ca, K, and Ti element intensities was carried out by X-ray fluorescence (XRF). The split halves of the gravity cores were measured by an ITRAX XRF Core Scanner (COX) equipped with a Cr-tube that was operated with 30 kV and 30 mA with a counting time of 15 seconds per step.

For the determination of Ca and Sr contents, discrete sediment samples were digested using a mixture of HNO_3, $HClO_4$, and HF in closed PDS-6 Teflon autoclaves at 180 °C (Heinrichs et al., 1986; Schnetger, 1997). The total acid digestions were fumed off three times with 6M HCl after evaporation on a hot plate at 180°C. Re-dissolved in 25 ml 2vol% HNO_3, the samples were measured by ICP-OES (iCAP 6300Duo, Thermo Fisher Scientific). Precision and accuracy of ICP-OES (<2.7% and <-3.3%) were determined by the international reference material SGR-1 (USGS).

4. Results

4.1 Age-depth model

Core MSM33/60-1GC comprises both the Holocene and the Eemian sapropels, which strongly contrast the glacial clayey intervals and thus assisted for a first stratigraphic assignment. As determined during earlier Black Sea studies focusing on the last 5,000 years of the penultimate glacial and the Eemian interglacial (Shumilovskikh et al., 2013a, b; Wegwerth

et al., 2014, 2018; Dellwig et al., 2019), increasing carbonate contents just before the onset of the Eemian sapropel at around 250-280 cm sediment depth (here presented by Ca/Ti_{XRF} ratios) clearly reflect the prominent Termination II warming (Fig. 2). From 668 cm down-core, we observed the same Ca/Ti_{XRF} pattern in cores MSM33/60-1GC, MSM33/57-1GC, and MSM33/56-1GC with the latter both extending much deeper than MSM33/60-1GC. Therefore, we combined the three gravity cores in order to construct a composite record covering a continuous and uninterrupted sequence over nearly the entire MIS 6 (130-184 ka BP). For inter-correlation of the cores, we used the high-resolution Ca/Ti ratios from XRF core scanning. Core MSM33/60-1GC comprises the youngest and largest part of MIS 6 including the transition (Termination II) to the last interglacial (Eemian, MIS 5e). Cores MSM33/57-1GC and MSM33/56-1GC extend the record down-core and their core depths were corrected/aligned relative to MSM33/60-1GC, which resulted in a total composite record length of 593 cm (207-800 cm composite depth; Fig. 2). Core MSM33/60-1GC contains three visible tephra layers, all of ca. 0.5 cm thickness, with the lowermost also identified in cores MSM33/57-1GC and MSM33/56-1GC (Figs. 2, 3).

Age tie points were derived from fine-tuning with other absolutely dated records using different geochemical parameters. For the youngest part of our record, i.e. Termination II and the Eemian (124-134 ka BP), we use the characteristic maxima and minima of sedimentary Sr/Ca, Ca, and $\delta^{18}O_{ostracods}$ presented during earlier studies with an already existing age model of core M72/5/22GC-8 (Fig. 4; Shumilovskikh et al., 2013a; Wegwerth et al., 2014). The probably most promising tool for age model construction of glacial Black Sea sediments is $\delta^{18}O_{ostracods}$ because it can be directly tuned to $\delta^{18}O$ records of the $^{230}Th/^{234}U$ dated speleothems from Northern Anatolian Sofular Cave covering large parts of the last 670 kyrs (here the individual speleothems So-4, So-6-3) (Fleitmann et al., 2009; Badertscher et al, 2011; Shumilovskikh et al., 2013a; Wegwerth et al., 2014). The speleothem record principally reflects the $\delta^{18}O$ signature of precipitation arriving from the Black Sea due to the water vapour source

effect (Badertscher et al., 2011). The strong similarity between $\delta^{18}O_{ostracods}$ and $\delta^{18}O_{Sofular\ Cave}$ during MIS 6 was therefore used for determination of 11 additional time markers between 160 and 184 ka BP (Fig. 4). The $\delta^{18}O_{ostracod}$ record from lowermost 65 cm probably covering parts of MIS 7 could not be stratigraphically assigned because it fails to mirror the characteristic three maxima seen in the $\delta^{18}O_{Sofular\ Cave}$ record (Badertscher et al., 2011).

Thanks to another well-dated speleothem flowstone record from Hungary (Abaliget Cave, ABA 1 and ABA 2; Koltai et al., 2017) showing similarity to our $\delta^{18}O_{ostracod}$ pattern, we could define further nine age markers between 131 ka BP and 160 ka BP, where the Sofular record has no data (Fig. 4). When compared to the Sofular speleothems, the $\delta^{18}O$ pattern from Abaliget speleothems shows a higher amplitude at least during the few time intervals they overlap (Badertscher et al., 2011; Koltai et al., 2017). A recent study explains this difference by the more continental position of the Abaliget Cave, where speleothems seem to archive rather the temperature variations and changes in moisture transport trajectories, whereas cave deposits from southern Europe (like Sofular Cave) seem to reflect mainly variations in the precipitation amount (Kern et al., 2018). Indeed, the Abaliget Cave record shows stronger variations between 145 and 135 ka BP than the $\delta^{18}O_{ostracods}$ record, although the general long-term trend is clearly visible and suitable for age model construction.

Independent time control is given by the eruption ages of two of the three macroscopic visible tephra layers in core MSM33/60-1GC. The uppermost tephra at 305 cm occurs close to the onset of the Eemian sapropel, and was described already in a previously investigated core M72/5/22GC-8 (Wegwerth et al., 2014). According to the age model presented in Wegwerth et al. (2014), the age of this ash layer is 130.9 ± 0.7 ka BP, which has been adapted here for the present age model. Because of its chronostratigraphic position a correlation of this tephra with the widespread P-11 Pantelleria eruption (~129-133 ka; Paterne et al., 2008; Rotolo et al. 2013; Satow et al., 2015) has been suggested but not geochemically confirmed (Wegwerth et al., 2014). This study provides new EPMA glass data for correlating this tephra from cores

MSM33/60-1GC, MSM33/61-1GC and M72/5/22GC-8, and the two underlying tephra layers from MSM33/60-1GC at 597 cm (and an equivalent sample from parallel core MSM33/61-1GC) and 678 cm depth (Fig. 3, Supplement file 2).

Accordingly, the uppermost, above-mentioned tephra has been identified as a mixed tephra layer that is located in all three cores at the MIS 6/5 transition. Respective samples MSM33/60-1GC–305 cm, MSM33/61-1GC–430 cm and M72/5/22GC-8–856 cm contain up to five distinct tephra glass populations (POP1 to POP5) that range from trachytic to high-silica rhyolitic compositions (Fig. 3). Glass chemical comparisons with well-known regional late MIS 6 tephra marker excluded a correlation with the P-11 tephra from Pantelleria and also did not reveal a clear match with any other prominent Mediterranean tephra marker from this time period. The latter comprise, for example, the phonolitic W-1 tephra from the Roman Volcanic Province (~138 ka; Bourne et al., 2015) and other MIS 5/6 tephras of Italian provenance that are recorded in key archives in Italy (Wulf et al., 2012) and in the Balkans (Leicher et al., 2016) (Fig. 3). However, some tentative assignments to volcanic provinces are possible, i.e. trachytic glass populations POP1 and POP2 likely derive from unknown eruptions from the Roman Volcanic Province and POP5 from a Campanian eruption in Italy. Rhyolitic glass populations POP3 and POP4 both possibly originated from Eastern Anatolian volcanoes (Schmincke and Sumita, 2014), with the higher silicic POP4 glass component likely deriving from the Nemrut Dagi volcanic system (Fig. 3).

The middle tephra occurs in core MSM33/60-1GC at 597 cm depth and in MSM33/61-1GC at 571 cm depth and matches the high-silica rhyolitic glass composition of the Kos Plateau Tuff (KPT) (Fig. 3), which is $^{40}Ar/^{39}Ar$ dated on land at 161 ± 2 ka (Smith et al., 1996; Bachmann et al., 2010). The radioisotopic age of the KPT agrees well with the modelled age of the speleothem tuned MSM33/60-1GC chronology at 159 ± 1.8 ka BP (Fig. 4).

The oldest tephra occurs in core MSM33/60-1GC at 678 cm depth and has a high-silica rhyolitic glass composition that is typical for central Anatolian tephras. In terms of glass

371 composition and chronostratigraphy it correlates best with the Upper Acigöl Tuff (UAT) from
372 Central Anatolia (Fig. 3). The UAT is (U-Th)/He zircon dated on land at 163 ± 7 ka (Schmitt
373 et al., 2011), which is in good agreement with the age of 167 ± 1 ka BP obtained by the tuned
374 MSM33/60-1GC chronology (Fig. 4).

375 According to the age model, the 1 cm sample resolution of the composite core averages
376 ~124 years. Mean squared estimates (MSEi) of age uncertainty were determined after Grant et
377 al. (2012) by considering four sensitive variables (radiometric dating error of speleothems,
378 sample spacing in the $\delta^{18}O_{speleothem}$ record, sample spacing in the $\delta^{18}O_{ostracods}$ record, and extra
379 uncertainty allowance for more ambiguous tie-points). The MSEi range between ± 0.7 ka and
380 ±1.8 ka (Fig. 4).

381 Overall, our new composite core extends to at least 184 ka BP, which allows to investigate
382 the climate and environmental conditions in the Black Sea "Lake" during almost the entire MIS
383 6, a period that experienced "one of the largest glaciations during the Late Quaternary" (Margari
384 et al., 2014; Colleoni et al., 2016; Hughes and Gibbard, 2018).

385

386 **4.2. Ostracod geochemistry and isotopic composition**

387 The predominant ostracod species identified in the composite core are *Candona* spp. and
388 *Bacuniella dorsoarcuata* (Zalanyi, 1929 in Boomer, 2012). Three additional species,
389 *Amnicythere* spp., *Loxoconcha* sp., and *Euxinocythere* sp., occur only sporadically and in minor
390 abundance (A. Stepanova; pers. comm.). *Candona* spp. is widely distributed in Black Sea
391 "Lake" sediments from the last and the penultimate glacial (e.g., Bahr et al., 2008; Boomer et
392 al., 2010; Wegwerth et al., 2014, 2016). *Bacuniella dorsoarcuata* occurs first only sporadically
393 but then in higher abundance and is most dominant (i.e. exceeding the abundance of *Candona*
394 spp.) between 168.5 ka BP and 180 ka BP. This species may have its origin in the Caspian Sea
395 (Olteanu, 1978; Boomer et al., 2005; Boomer, 2012; Richards et al., 2017). Since ca. 127 ka

BP, ostracods disappear due oxygen depletion within the course of the Mediterranean-Black Sea reconnection and Eemian sapropel formation (Wegwerth et al., 2014, 2018).

The ostracod $\delta^{18}O$ values range between +1.5 ‰ and -12.2 ‰ (Fig. 5A) and the record shows three distinct intervals with pronounced negative excursion becoming less negative from the oldest towards the youngest interval, namely at 180-167 ka BP (min. -12.2 ‰), 160-145 ka BP (min. -10.8 ‰), and 133-130 ka BP (min. -8.3 ‰). The $\delta^{18}O_{ostracods}$ reach higher values between 160 and 167 ka BP (max. -1.9 ‰) and around 145 ka BP (max. -4.0 ‰) and are relatively comparable with the level during T II (max. -1.2 ‰).

For the element/Ca ratios of the ostracods, we also calculated a 3-point moving average to reduce noise and prevent overvaluation of single data points. In contrast to the $\delta^{18}O_{ostracods}$, the element/Ca ratios fluctuate much stronger and reveal a remarkable short-term variability. The $Mg/Ca_{ostracods}$ values range between 1.3 and 9.3 mmol mol^{-1} (Fig. 5B). In addition to T II, $Mg/Ca_{ostracods}$ values also increase during the first half of MIS 6 at around 177 ka BP, 173 ka BP, and 160 ka BP. The penultimate glacial average of $Mg/Ca_{ostracods}$ of about 2 mmol mol^{-1} is comparable with values measured for the last glacial period within MIS 2 (Bahr et al., 2008). The $Mg/Ca_{ostracods}$ amplitude of 2 mmol mol^{-1} during MIS 6 is nearly the same as during MIS 3 (Wegwerth et al., 2015).

The $Sr/Ca_{ostracods}$ ranges between 0.6 and 2.4 mmol mol^{-1} and shows a more stable pattern when compared to $Mg/Ca_{ostracods}$ (Fig. 5C). The strong increase of $Sr/Ca_{ostracods}$ from 0.9 to 2.4 mmol mol^{-1} during T II is again associated with the Mediterranean-Black Sea reconnection (Wegwerth et al., 2014). Furthermore, there are distinct long intervals during MIS 6 showing higher values of up to 1.5 mmol mol^{-1} around 183, 165, 161, 149, 135 and 130 ka BP. During these periods, $Sr/Ca_{ostracods}$ increases sharply and decreases gradually back to the average value (except for T II). The long-term trend of the $Sr/Ca_{ostracods}$ record mimics the $\delta^{18}O_{ostracods}$ pattern with lower levels at 179-165 ka BP, 158-150 ka BP and around 137 ka BP and 132 ka BP. The

421 $Sr/Ca_{ostracods}$ amplitude during MIS 6 of 1.2 mmol mol^{-1} is much higher than the 0.4 mmol mol^{-1} during MIS 3 (Wegwerth et al., 2016).

423 The $^{87}Sr/^{86}Sr_{ostracods}$ values range between 0.708612 and 0.709405 (average 0.708951; n=33; Fig. 5D) and strongly exceed the last glacial maximum level of 0.7091 (Major et al., 2006) during 153-147 ka BP and 133-130 ka BP with the latter also observed during a previous study by Wegwerth et al. (2014). Despite the low sampling resolution it becomes obvious that $^{87}Sr/^{86}Sr_{ostracods}$ exceeds the last glacial maximum level not only during T II but also in general since 160 ka BP. In contrast, during the first half of MIS 6 (184 - 160 ka BP), $^{87}Sr/^{86}Sr_{ostracods}$ are generally on a lower level and even fall below values determined for the last glacial.

430 Apart from ostracods, the wet-sieved fraction >150 µm contains coastal ice-rafted detritus (IRD_C), whose abundance relates to coastal ice formation and winter strength (Nowaczyk et al., 2012; Wegwerth et al., 2015). The content of IRD_C ranges between 0 and 350 grains per cm^3 (Fig. 5E). IRD_C shows a distinct millennial-scale variability throughout the record. Very high abundances are counted during 183-179 ka BP and longer periods of very low or even absent IRD_C are seen during 179-174 ka BP and during 130-124 ka BP.

436

437 **4.3. Sediment geochemistry**

438 The content of total inorganic carbon (TIC) remains on a comparatively low level of 1.5% during almost the entire MIS 6 (Fig. 5F). There are only few short periods with increasing carbonate where TIC contents up to 2.5% at 184 ka BP, 2.9% at 167 ka BP, and about 4% during T II are observed. During the Eemian, TIC reaches up to 8.9%. The background level of 1-1.5% TIC during large parts of the record represents most likely detrital carbonate, similar as determined for glacial and stadial periods (ave. 1.6% TIC) during earlier studies e.g. via microscopy in the Black Sea (Bahr et al., 2008; Shumilovskikh et al., 2012; Wegwerth et al., 2014, 2015). The TIC content above the detrital background level during the aforementioned periods is similar to the conditions during MIS 3–interstadials and terminations in the Black

Sea (3-4.5%) and most likely reflects increased authigenic carbonate precipitation due to phytoplankton productivity, which is supported by increased Ca/Ti_{XRF} values during the same periods (Fig.2). Although the TIC variability during MIS 6 remains low, a trend to generally higher TIC is evident for the second half of MIS 6. Thus excluding the aforementioned periods with slightly higher TIC, the average TIC during the first part of MIS 6 (170-180 ka BP) is 1%, while it is 1.6% during the second part (132-160 ka BP).

With an average value of 0.3%, total organic carbon (TOC) is very low during MIS 6 (Fig. 5G). Unlike TIC, TOC is higher during the first half of MIS 6 revealing a maximum value of 0.46%. Interestingly, the pattern of TOC during 179-169 ka BP strongly equals the morphology of a typical interstadial during MIS 3 (Wegwerth et al., 2016), with abruptly increasing and gradually decreasing TOC. In contrast to MIS 3, however, this period lasted much longer (10 ka) than the MIS 3 interstadials (< 3 ka). TOC also shows slightly higher values around 184 ka BP (0.35%) and around 167 ka BP (max. 0.38%). During the second half of MIS 6, TOC reaches not more than 0.31% but shows abruptly increasing values to about 10% at the onset of the Eemian (Wegwerth et al., 2018).

The K/Ti_{XRF} shows a maximum during 169-147 ka BP and 138-130 ka BP, and at 128 ka BP, and at 125 ka BP (Fig. 5H). During the first part of MIS 6, K/Ti_{XRF} ratios are generally on a lower level when compared to the second part. To a certain degree, it seems that K/Ti_{XRF} follows the pattern of $^{87}Sr/^{86}Sr_{ostracods}$, although both are presented in a different sampling resolution.

5. Discussion

The $\delta^{18}O_{ostracod}$ record from the SE Black Sea documents pronounced hydrological changes within the course of substantial climate variations during MIS 6. The variations in the $\delta^{18}O$ incorporated from the surrounding water into the carbonate shells is the result from changes in ambient temperature during ostracod growth and from changes in $\delta^{18}O$ of Black Sea

water itself. The latter is influenced by a) the changes of the oxygen isotopic composition of direct precipitation in turn depending on its condensation temperature, b) the oxygen isotopic composition of rivers entering the Black Sea "Lake" depending in turn on the composition of rainfall or of other freshwater sources like meltwater, and c) lake surface evaporation (e.g. van Grafenstein et al., 1999; Bahr et al., 2006; van Hardenbroek et al., 2018). Mediterranean water as an additional source for changing $\delta^{18}O_{ostracod}$ can be excluded because the sea level was below the Bosporus sill depth (-35 m) during the entire MIS 6 (Fig. 6B; Grant et al., 2012), preventing the inflow of saltier Mediterranean Sea water.

Three distinct periods with considerably depleted values are clearly visible in the present $\delta^{18}O_{ostracod}$ record (Fig. 5A; 180-167 ka BP, 160-145 ka BP, and 133-130 ka BP). Considering a maximum amplitude of 13.7‰ in the $\delta^{18}O_{ostracod}$ record, temperature changes as the main trigger for variations in $\delta^{18}O_{ostracod}$ are not compatible with a decrease of about ~0.25‰ in $\delta^{18}O$ per rise of about ~1°C (e.g., McCrea, 1950; Epstein et al., 1953). Since $\delta^{18}O_{ostracod}$ values generally increase during humid periods in the course of Terminations I and II, direct rainfall over the Black Sea as a source for the enormous negative oxygen isotope excursion can be excluded as well. Therefore, the variations in the $\delta^{18}O_{ostracod}$ record most likely reflect changes in isotopic signature, amounts, and sources of river discharge into the Black Sea "Lake".

As already demonstrated by earlier studies, negative excursions of $\delta^{18}O_{ostracod}$ in Black Sea "Lake" sediments suggest high contribution of isotopically light meltwater originating from the disintegrating Fennoscandian Ice Sheet (Major et al., 2006; Bahr et al., 2008; Wegwerth et al., 2014). Considering the last glacial, when $\delta^{18}O_{ostracod}$ values were not lower than -6.8‰ (Bahr et al., 2006), the depletions during the three periods of MIS 6 with minimum values ranging between -8.3‰ and -12.2‰, imply either a significantly higher amount of isotopically depleted water and/or a contribution of water that was isotopically more depleted than during the last glacial. The negative excursion during Termination II resulted most likely from a Black Sea meltwater pulse at the end of the penultimate glacial divided into the substages BSWP-II-1

(133.5–132.5 ka BP) and BSWP-II-2 (131.5–130.5 ka BP; Shumilovskikh et al., 2013a; Wegwerth et al., 2014). During this period, $\delta^{18}O_{ostracod}$ varied in concert with $\delta^{18}O_{Sofular\ Cave}$ due to the water vapour source effect identifying the Black Sea as the main source for the Sofular Cave speleothem growth (Lachniet, 2009; Badertscher et al., 2011; Wegwerth et al., 2014). Such similarity between the $\delta^{18}O_{ostracod}$ and $\delta^{18}O_{Sofular\ Cave}$ records is also evident during the first half of MIS 6 (180-167 ka BP), which corroborates a long-term and even stronger period of meltwater discharge owing to the considerably larger Eurasian ice volume (Svendsen et al., 2004; Colleoni et al., 2009; Badertscher et al., 2011; Marks et al., 2018). A similar scenario with strong meltwater supply is also conceivable for the second period of oxygen isotope depletion in the Black Sea "Lake" (160-145 ka BP), where the record of Sofular Cave bears a gap (Badertscher et al., 2011). In particular, this second period falls within the time window of the well-known massive 'Fleuve Manche' (Channel River) palaeoriver discharge from the Fennoscandian Ice Sheet into the Bay of Biscay that occurred between 160 ka BP and 150 ka BP (Toucanne et al., 2009; Boswell et al., 2019) and is possibly recorded in the Black Sea "Lake" sediments as well. The identification of this meltwater period in the Black Sea would imply that the meltwater discharge occurred not only by one mega-river system as assumed so far (e.g., Penaud et al., 2009), but was accompanied by a notable eastern European drainage component.

We hypothesise that variations in the volume and extent of the Eurasian Ice Sheet along with associated changing atmospheric circulation patterns affected the hydrological conditions in the glacial Black Sea "Lake" to a vast extent. In the following, we will concentrate on the hydrological conditions during the individual periods in more detail for identification of potential meltwater pulses and pathways. According to the nomenclature by Soulet et al. (2013), we will refer to the three Black Sea water pulse periods as BSWP with the first two during MIS 6, BSWP-6-1 and BSWP-6-2, and those that occurred during Termination II, BSWP-II-1 and BSWP-II-2, as already discussed by Wegwerth et al. (2014). BSWP-6-1 occurred prior to the

larger Drenthe ice advance (175-160 ka BP) and BSWP-6-2 prior to the smaller Warthe ice advance (150-140 ka BP) (Ehlers et al., 2011).

5.1 BSWP-6-1, 180-167 ka BP (MIS 6e-d)

The transition from the warmer MIS 7 to the colder MIS 6 at 191 ka BP involved a decreasing global sea level (Lisiecki and Raymo, 2005) that most likely caused a separation of the Black Sea from the Marmara/Mediterranean Seas at ca. 189 ka BP (Badertscher et al., 2011). There is no evidence for remnant saline-brackish and oxygen-deficient bottom water conditions at 184 ka BP, typically characterising at least the last two interglacials in the Black Sea associated with a connection to the Mediterranean Sea (e.g., Wegwerth et al., 2018; Dellwig et al., 2019). This suggests that desalinisation/freshening and oxygenation of the potentially former oxygen-deficient and saline-brackish Black Sea water column occurred within less than 5,000 years. Otherwise, a stronger outflow regime during that time could have subdued the inflow of salty Mediterranean water via the Bosporus strait. Between ca. 193 ka BP and 183 ka BP, the northern hemispheric summer insolation decreased (Berger and Loutre, 1991), the Eurasian Ice Sheet volume increased (Bintanja and van de Wal., 2008), and temperatures in the North Atlantic/western Mediterranean Sea decreased to a level comparable to the transition from MIS 5 to MIS 4 (Martrat et al., 2004, 2007).

During the period from the onset of our Black Sea "Lake" record at 184 ka BP to 173 ka BP, northern hemisphere summer insolation increased and the Eurasian Ice Sheet volume decreased accordingly (Fig. 6A, C; Berger and Loutre, 1991; Bintanja and van de Wal., 2008). A northward shift of the atmospheric polar front and the ITCZ likely caused higher rainfall due to stronger Mediterranean cyclones in the mid-latitudes (e.g., Ayalon et al., 2002; Bard et al., 2002; Penaud et al., 2009; Regattieri et al., 2014). Interstadial-like warming phases during MIS 6 are inferred from a $\delta^{18}O$ record of a synthetic Greenland ice core (Fig. 6D; Barker et al., 2011) and from alkenone-based sea surface temperature reconstructions in the North

Atlantic/Mediterranean region (Fig. 6E; Martrat et al., 2004, 2007). Temporary milder conditions in the Black Sea region during the onset of MIS 6, as determined by elevated $Mg/Ca_{ostracod}$ values (Fig. 6F), suggest stadial to interstadial temperature variations for the deeper Eurasian continent as well. There are two short-term periods at around 177 ka BP and 173 ka BP, when $Mg/Ca_{ostracods}$ increases of about 1.5 to 2 mmol mol^{-1} (Fig. 6F). According to Bahr et al. (2008), such an increase in $Mg/Ca_{ostracods}$ would correspond to a mean annual temperature rise of about 1.5 to 4°C in bottom waters. Similar temperature changes were determined from a Black Sea "Lake" $Mg/Ca_{ostracods}$ record comprising DO cycles during MIS 3 (Wegwerth et al., 2015). During the same time, the abrupt disappearance of IRD_C (Fig. 5E) indicates milder winter conditions without coastal ice formation, thus suggesting, in addition to the higher $Mg/Ca_{ostracods}$ ratios, a generally warmer climate. Although not as high as during MIS 3 interstadials (Wegwerth et al., 2015, 2016), slightly increasing TOC and TIC contents may indicate a response of higher productivity and autochthonous carbonate formation to warming (Fig. 5F, G).

The retreat of the Eurasian Ice Sheet between 183 ka BP and 173 ka BP (Bintanja and van de Wal, 2008) likely caused, apart from a rising global sea level of about 20 m (Grant et al., 2012), meltwater discharge from the Eurasian Ice Sheet towards the Caspian and Black Seas (Fig. 6B, C; Badertscher et al., 2011). The period from 180-167 ka BP in the studied sediments bears the most negative $\delta^{18}O_{ostracod}$ excursion during MIS 6 pointing to an extensive meltwater release into the Black Sea "Lake" (Fig. 6H). Since this period spans about 13 kyrs, we suggest a continuous and long-lasting discharge of meltwater. The input of meltwater caused a decline of about 8‰ in the $\delta^{18}O_{ostracod}$ record, which corresponds to a decline of about 7‰ in the $\delta^{18}O_{Sofular\ Cave}$ record (Fig. 6G, H). Although the Sofular speleothem record is not complete for the entire Pleistocene, it seems that this meltwater phase was one of the strongest during the last 670 ka BP since the $\delta^{18}O_{Sofular\ Cave}$ record reveals the most negative excursion at the same time (at ca. 176 ka BP; Badertscher et al., 2011). Regarding the pronounced and long-term

577 negative excursion in both $\delta^{18}O$ records, considerable amounts of meltwater input probably
578 resulted in a lake-level rise. A presumably higher lake level during the meltwater period likely
579 generated new shallow water depositional space and increased the distance of the core location
580 relative to its terrestrial sources (i.e. Anatolia), both factors explaining the reduced
581 sedimentation rates (Fig.4). Whether such a potential lake level rise was even associated with
582 an overspill through the Bosporus strait into the Marmara and Mediterranean Seas remains
583 elusive. Although resulting from humid conditions instead of meltwater input, lake-level rise
584 associated with Black Sea "Lake" spill-out was supposed for the last glacial during periods of
585 MIS 3 (Çağatay et al., 2009; Aloisi et al., 2015; Çağatay et al., 2015; Wegwerth et al., 2016).
586 A lake-level rise of at least 100 m is suggested for the Termination I meltwater pulse, which
587 was associated with a decline of only 1‰ in the Black Sea $\delta^{18}O$ (Bahr et al., 2006; Soulet et al.,
588 2013). Given the much stronger negative excursion in the $\delta^{18}O$ ostracod records with a decline
589 of about 8‰ and the longer time span during BSWP-6-1, we expect that a much larger volume
590 of meltwater entered the Black Sea "Lake" resulting in a considerable lake-level rise and
591 potentially in a spill-out into the Mediterranean Sea.

592 Owing to a residual salinity of about 7 to 12 ‰ during the last two glacials in the Black
593 Sea "Lake" (Shumilovskikh et al., 2013a), that derives from preceding connections to
594 Mediterranean Sea, it is possible to detect changes in salinity caused by freshening
595 (rainfall/riverine discharge, meltwater) or evaporation in the lacustrine sediments. A promising
596 proxy for estimation of changes in salinity is the $Sr/Ca_{ostracods}$ ratio because the uptake of Sr into
597 the ostracod´s carbonate shell is related to salinity and the Sr concentration in the host water,
598 respectively (Chivas et al., 1986; Engstrom and Nelson, 1991; Wansard et al., 1998).
599 $Sr/Ca_{ostracods}$ show lowest values between 179 and 166 ka BP corresponding to BSWP-6-1 and
600 confirming an elevated freshwater input (Fig. 5C). The average $Sr/Ca_{ostracods}$ ratio of 0.9 mmol
601 mol^{-1} during that period is comparable with $Sr/Ca_{ostracods}$ values during meltwater pulses during
602 Termination I and II (Bahr et al., 2008; Wegwerth et al., 2014) implying similar bottom water

603 salinities. That would imply that similar amounts of meltwater entered the Black Sea "Lake"
604 during the terminations and BSWP-6-1 contrasting to the suggestion of a much larger volume
605 of meltwater during BSWP-6-1 as emerged from the $\delta^{18}O_{ostracods}$ signature. Considering,
606 however, the strongest retreat of the Eurasian Ice Sheet volume during MIS 6 that coincides
607 with BSWP-6-1 (Fig. 6C; Bintanja and van de Wal, 2008), we maintain the suggestion of larger
608 meltwater amounts during BSWP-6-1 and possibly less sensitivity of ostracod shells to slight
609 variations in Sr/Ca_{water}.

610 According to Badertscher et al. (2011), the meltwater during the early MIS 6 (166.8 ka
611 BP- 182.2 ka BP) ultimately originated from the Caspian Sea and entered the Black Sea "Lake"
612 via the Manych Depression (Fig. 1). The Caspian Sea, in turn, was fed by river Volga due to
613 the melting of the Fennsoscandian Ice Sheet that was ca. 56% larger and extended considerably
614 wider into the Eurasian continent than during the last glacial (Svendsen et al., 2004; Colleoni
615 et al., 2016; Hughes and Gibbard, 2018; Marks et al., 2018). Regarding the general distribution
616 of $\delta^{18}O$ in precipitation over Eurasia with strongest isotopic depletion over an area of the former
617 eastern Eurasian Sheet (e.g. Badertscher et al., 2011), the pronounced negative values in the
618 $\delta^{18}O_{ostracods}$ may not only point to large amounts of meltwater but also to its origin along the
619 eastern Eurasian Ice Sheet. The most southern ice sheet component, the Dnieper lobe close to
620 the Black Sea being absent during the last glacial (Svendsen et al., 2004), played possibly the
621 most important role bridging the Eurasian Ice Sheet and the Caspian Sea-Black Sea drainage
622 system. The minimum volume of the Eurasian Ice Sheet (Bintanja and van de Wal, 2008) during
623 MIS 6, which corresponds to the maximum summer insolation at 65°N (Berger and Loutre,
624 1991), would be in line with enhanced meltwater supply to the Caspian and Black Seas (Fig.
625 6B, C). The dominance of the Caspian ostracod species *Bacuniella dorsoarcuata* (Boomer et
626 al., 2005; Boomer, 2012; Richards et al., 2017) in the Black Sea during that period corroborates
627 the suggested communication between the Black and Caspian Seas, as long as this is not a
628 remnant species from the preceding Caspian overflows. Further faunal evidence for water

intrusions from the Caspian Sea into the Black Sea comes from Caspian mollusc assemblages detected in Black Sea sediments during that time (Zubakov, 1988). A preliminary study of dinoflagellate assemblages from selected samples of the Black Sea cores revealed occurrence of *Caspidinium rugosum* (Marret et al., 2004) confirming a connection between the Caspian and Black Seas during that period as well (L. Shumilovskikh; pers. comm.).

In addition to the river Volga, the rivers Don, Dnieper, Dniester, and Danube may have contributed directly to the enhanced meltwater supply in the Black Sea "Lake". A promising proxy for the assessment of meltwater pathways and sources for the glacial Black Sea forms the Sr-isotope signature of (ostracod) carbonate shells ($^{87}Sr/^{86}Sr_{ostracods}$). An advantage of $^{87}Sr/^{86}Sr_{ostracods}$ is the fact that it is unaffected by temperature and/or biogenic fractionation, but can reflect the catchment geology and depends on the respective drainage region (Reinhardt et al., 1998; Major et al., 2006). The $^{87}Sr/^{86}Sr_{ostracod}$ values decrease strongly from 0.709033 to 0.708612 implying main freshwater supply and its mixing within the Black Sea "Lake" within approximately 7,500 years from 183.6 to 176.1 ka BP (Fig. 6I). Remarkably, the value of 0.709033 at ca. 183.6 ka BP prior to meltwater supply is slightly lower than the modern Black Sea value, which is about 0.709120-0.709133 (Table 1; Major et al., 2006; Ankindinova et al., 2019). Although other proxies, like the low $Sr/Ca_{ostracods}$ values, would exclude a connection to the Mediterranean Sea, the high radiogenic Sr-isotope level likely reflects a preceding Mediterranean-Black Sea connection. According to Badertscher et al. (2011), such connection may have indeed prevailed at 188.9 ka BP – 198.7 ka BP and 202.1 ka BP – 215.0 ka BP.

During the BSWP-6-1, $^{87}Sr/^{86}Sr_{ostracods}$ show relatively low values (0.708612-0.708747) being much less radiogenic compared to the meltwater periods during Terminations I and II (Table 1; Major et al., 2006; Wegwerth et al., 2014). Since freshwater contribution by rainfall alone would not change the Sr-isotopic composition of the Black Sea "Lake", the decrease of the $^{87}Sr/^{86}Sr_{ostracods}$ during that period points to enhanced riverine supply. Potential rivers with similar low present day $^{87}Sr/^{86}Sr$ ratios, which directly enter the Black Sea, would be the

Dnieper and Don (Table 1). For river Dniester $^{87}Sr/^{86}Sr$ are not available and $^{87}Sr/^{86}Sr$ values from Danube and Sakarya are above the level during BSWP-6-1 (Table 1). Thus, in addition to the river Volga and the Caspian Sea, freshwater runoff by Dnieper and Don could explain the decrease of the $^{87}Sr/^{86}Sr_{ostracods}$. The Dnieper lobe represented the south-eastern flank of the Eurasian Ice Sheet at ~50°N, close to the Black Sea (Svendsen et al., 2004; Ehlers and Gibbard, 2007; Marks et al., 2018; Fig. 1). Therefore, we assume that the freshwater contribution occurred not only via the Caspian Sea, but also by meltwater from the Dnieper lobe during its retreat probably in combination with drainage of a large ice-dammed lake south of the ice sheet margin (Svendsen et al., 2004; Lang et al., 2018).

As figured out earlier for the last glacial (MIS 3), K/Ti ratios may help for estimation of the amount and source of riverine input (Wegwerth et al., 2016). The rise of K relative to Ti would point to an enhanced supply of detrital suspended matter predominantly via the northern and western rivers Danube, Dniester and Dnieper (Piper and Calvert, 2011). During BSWP-6-1, K/Ti is very low suggesting reduced discharge from the northern and western rivers, except for slight increases during two short periods (179-176 ka BP, 172-171 ka BP, Fig. 5H). Regarding a modern oxygen isotope composition of -10.5‰ (VSMOW) for the river Danube (Özsoy et al., 2002) and a decrease to <-12‰ (VPDB) during BSWP-6-1, Danube discharge alone could not account for the $\delta^{18}O_{ostracod}$ depletion. Along with the very low radiogenic Sr-isotope signature in the ostracods and the high abundance of ostracods of Caspian origin, we suggest that the largest amount of meltwater into the Black Sea passed through the Caspian Sea during BSWP-6-1.

5.2 Meltwater interruption 167-160 ka BP (MIS 6d-c)

The insolation decrease since 173 ka BP, which reached a minimum at ca. 160 ka BP, involved the re-expansion of the Eurasian Ice Sheet during the Drenthe ice advance, a decreasing global sea level, and a southward shifting atmospheric polar front associated with

cooling and reduced rainfall (Fig. 6A-C; Berger and Loutre, 1999; Bintanja and van de Wal., 2008; Grant et al., 2012). Starting at ca. 170 ka BP, $\delta^{18}O_{ostracod}$ increased within 4,000 years from -12‰ to -2‰ implying major hydrological changes associated with an interruption of meltwater discharge due to ice sheet expansion (Fig. 6H). Although, this period was associated with long-term cooling and ice sheet expansion in northern Eurasia, frequent changes in TIC, TOC, and IRD_C contents suggest stadial to interstadial conditions with three periods of higher productivity and milder winters (Fig. 5E-G).

At ca. 164 ka BP and 161 ka BP, enhanced $Sr/Ca_{ostracods}$ point to a salinity rise in the Black Sea "Lake" (Figs. 5C), most likely due to the meltwater disruption and enhanced evaporation exceeding riverine freshwater supply. The asynchronous pattern between $\delta^{18}O_{ostracod}$ and $Sr/Ca_{ostracod}$ possibly resulted from cessation of meltwater discharge prior to increased evaporation. The two discrete peaks of $Sr/Ca_{ostracod}$ co-occur with rising $Mg/Ca_{ostracod}$, which is roughly synchronous with the Greenland interstadials (Figs. 5B, C, 6D; Barker et al., 2011). The increased sedimentary K/Ti and higher radiogenic $^{87}Sr/^{86}Sr_{ostracod}$ values of up to 0.708843 at 162 ka BP point to riverine discharge mainly by the Danube River (Figs. 5H, 6I). The higher $^{87}Sr/^{86}Sr_{ostracod}$ values indicate a separation from the Caspian Sea and reduced riverine discharge from the river Dnieper being in line with an expanded Eurasian Ice Sheet and meltwater disruption.

5.3 BSWP-6-2, 160-145 ka BP (MIS 6c-b)

Since ca. 160 ka BP, the northern summer insolation increased and reached its maximum at ca. 148 ka BP, but was below that during the early MIS 6 at ca. 174 ka BP (Fig. 6A; Berger and Loutre, 1991). The insolation changes likely caused a shrinking Eurasian Ice Sheet again and a moderately increasing global sea level (Fig. 6B, C; Bintanja and van de Wal., 2008; Grant et al., 2012). DO-like climate variability may have been subdued and in a long-term view,

temperature decreased by about 6°C in the North Atlantic/western Mediterranean region (Fig. 6D, E; Barker et al., 2011; Martrat et al., 2004, 2007).

In the Black Sea "Lake", the second large meltwater period during MIS 6 between 160 ka BP and 145 ka BP (BSWP-6-2) was similar in duration to BSWP-6-1, but accompanied by somewhat different environmental conditions. Although the BSWP-6-2 falls within the period of a high insolation, $Mg/Ca_{ostracod}$ and IRD_C imply rather cold glacial conditions in the Black Sea region, which strongly contrasts to the milder conditions during BSWP-6-1 (Figs. 6A, F, 5E). The very low TOC and TIC contents in the sediment point to reduced productivity, most likely because of the colder conditions (Fig. 5F, G). This situation with subdued climate variability is comparable to the late MIS 3-MIS 2 situation in the Black Sea "Lake", when insolation was on a similar level (Laskar et al., 2004; Wegwerth et al., 2015, 2016). The $\delta^{18}O_{ostracod}$ record during BSWP-6-2 shows a pronounced negative excursion with values up to -10‰ (VPDB; Fig. 6H). When compared to BSWP-6-1, showing an excursion up to -12‰ (VPDB), slightly lower amounts of meltwater likely entered the Black Sea "Lake" during BSWP-6-2, which is in line with a lower retreat and volume loss of the Eurasian Ice Sheet compared to BSWP-6-1 (Fig. 6C; Bintanja and van de Wal., 2008). The decreasing $Sr/Ca_{ostracods}$ ratios suggest a lowered salinity, but that was not as low as during BSWP-6-1 (Fig. 5C). Throughout this period of meltwater release into the Black Sea "Lake", the $^{87}Sr/^{86}Sr_{ostracod}$ values are above 0.709044 (max. 0.709207) and are much more radiogenic than during the first MIS 6 meltwater period (Fig. 6I). This finding strongly suggests different meltwater sources and drainage pathways during both the BSWPs. Although a Caspian overflow to the Black Sea was also suggested during BSWP-6-2 (Arkhipov et al., 1995; Svitoch et al., 2000), such conditions are not compatible with the considerably heavier Sr-isotope signature. Evidence indicates that the Eurasian Ice Sheet configuration differed strongly during BSWP-6-1 and BSWP-6-2. While the Eurasian Ice Sheet was separated into a Fennoscandian and a British Irish Ice Sheet during BSWP-6-1, both Ice Sheets were connected during BSWP-6-2 (Penaud et al.,

2009). This likely caused diverging meltwater pathways and may explain why the imprint of meltwater discharge during BSWP-6-2 is stronger in Western Europe than BSWP-6-1, which was possibly stronger in Eastern Europe as reflected in Black Sea "Lake" $\delta^{18}O_{ostracod}$ record. The pronounced retreat of the Eurasian Ice Sheet at the beginning of MIS 6 may also have produced large ice-dammed lakes at the ice sheet margins (Lang et al., 2018). BSWP-6-2 (160-145 ka BP) occurred nearly during the same time as the massive 'Fleuve Manche' (Channel River, 160-150 ka BP) palaeoriver discharge from the Fennoscandian Ice Sheet into the Bay of Biscay (Penaud et al., 2009; Toucanne et al., 2009; Boswell et al., 2019). The identification of a coeval meltwater event in the Black Sea suggests that the meltwater discharge occurred not only by one mega-river system draining into the Atlantic as assumed so far (e.g., Penaud et al., 2009), but was accompanied by an eastern European drainage component draining into the Caspian Sea–Black Sea–Mediterranean Sea corridor. At the same time, alpine ice melting (Piva et al., 2008; Toucanne et al., 2009) may have amplified freshwater supply into the Black Sea "Lake" from the Danube drainage area, possibly resulting in pronounced variations in the Black Sea "Lake" level. A higher Danube contribution is supported by the slightly lower negative $\delta^{18}O$ excursion (containing less negative values compared to Volga) and higher K/Ti ratios (Figs. 6H, 5H).

As mentioned above, the most striking difference between both large BSWPs is the Sr-isotope signature with much higher radiogenic values during BSWP-6-2 (0.709044-0.709207). Similar and even higher $^{87}Sr/^{86}Sr_{ostracods}$ values were determined in another gravity core (Wegwerth et al., 2014) and in the present study for BSWP-II during Termination II coinciding with Heinrich event 11. Apart from both meltwater periods during MIS 6 (BSWP-6-2 and BSWP-II), such highly radiogenic Sr-isotope values were not detected during any other time slices throughout the late Pleistocene and Holocene in the Black Sea so far (Major et al., 2006; Yanchilina et al., 2017; Ankindinova et al., 2019). Sr-isotope data from Miocene and Pliocene sediments in the Paratethys show also much lower values than those recorded here during MIS

6 (Table 1; Vasiliev et al., 2010; Van Baak et al., 2019). The available present day Sr-isotope data of rock and sediment sources from the Black Sea drainage areas as well as the rivers entering the Black Sea show values that are far too low for explaining the high radiogenic values during BSWP-II and BSWP-6-2 meltwater periods (Table 1). Both, rocks in the Anatolian/Pontic Mountains and Caucasus have $^{87}Sr/^{86}Sr$ values <0.7054 (Mengel et al., 1987; Lebedev et al., 2007; Altherr et al., 2008; Aydin et al., 2008; Kaygusuz and Aydınçakır, 2009).

A study presenting Sr-isotope data of modern and Holocene mollusc shells from the Baltic Sea shows high radiogenic Sr values like our Black Sea ostracods, which are explained by the high radiogenic Sr isotope signature of Precambrian rocks along the Scandinavian craton (modern: av. 0.709566, n=19; subfossil (6.6-3.2 ka BP): 0.709306, n=16; Table 1; Widerlund and Andersson, 2006). However, these data represent Holocene values and reflect the large amounts of modern riverine input in the Baltic Sea. Today, rivers draining the Precambrian Shield show a Sr-isotope signature >0.725 (Négrel et al., 2005). During MIS 6, however, the Scandinavian craton was completely covered by ice (Svendsen et al., 2004). In that case, erosion and weathering was likely strongly reduced in that region preventing the export of the high radiogenic Sr-isotope signature to the Black Sea. Therefore, the meltwater arriving at the Black Sea most likely originated from the ice sheet margins and ice-dammed lakes on the east European platform, where mostly Phanerozoic material with lower Sr-isotope values is exposed (Widerlund and Andersson, 2006). During the same period of BSWP-6-2, considerable amounts of meltwater entered the Bay of Biscay (Toucanne et al., 2009), which was potentially associated with ice sheet retreat along the margins of the Fennoscandian craton. Low amounts of water draining small parts of that high radiogenic region could have been sufficient to account for a high radiogenic signature of water draining into the Black Sea region. Nevertheless, since records of other time slices of meltwater release into the Black Sea originating from the Fennoscandian Ice Sheet show much lower $^{87}Sr/^{86}Sr$ values, other sources must have contributed high radiogenic Sr-isotope water to the Black Sea during BSWP-6-2.

Previously, Wegwerth et al. (2014) hypothesised that the high radiogenic $^{87}Sr/^{86}Sr_{ostracods}$ signature for the T II meltwater pulse (0.709452) derived from a Himalayan freshwater source because streams draining the Lesser Himalaya have a very high radiogenic Sr-isotope composition (Table 1; Henderson et al., 1994; Jacobson et al., 2002). More precisely, it was suggested that the Amu Darya was fed by Himalayan rivers carrying high Sr-radiogenic water directly to the Caspian Sea, which in turn entered the Black Sea via the Manych Depression (Wegwerth et al., 2014). Although the modern Amu Darya drains into the Aral Sea, its channel seems to have changed the direction several times and was even connected to the Caspian Sea via the Lake Sarykamysh and the Uzboy Channel (Boomer et al., 2000; Boomer, 2012). A detailed history of the different courses of the various rivers in the Aral-Caspian region is given by Boomer et al. (2000) and references therein. Sr-isotope data from the drainage basin of the Caspian and Aral Seas are rare, but the high radiogenic value of 0.70940 of the Syr Darya (Pokrovsky et al., 2017) likely corroborates our suggestion of a freshwater source in the western Himalaya. The Syr Darya is fed by the rivers Naryn and Qoradaryo originating from the Tian Shan Mountains in Kirgizstan (Pokrovsky et al., 2017; Burr et al., 2019). The Amu Darya originates from the Pamir Mountains. Both rivers carried glacier meltwater from the Tian Shan and Pamir Mountains and formed the modern Aral Sea (Burr et al., 2019). The loess from Tian Shan contains high radiogenic $^{87}Sr/^{86}Sr$ values and is a source for Syr Darya and Amu Darya, which explains the high values at least for Syr Darya (no data are available for Amu Darya) (Pokrovsky et al., 2017 and references therein). Here we refine our previous hypothesis and propose that a potential source for the high radiogenic Sr during BSWP-6-2 and BSWP-II were loess deposits and riverine meltwater from the Tian Shan (and probably Pamir) mountains. We suggest that this meltwater, carrying the high radiogenic Sr, reached the Black Sea via Syr Darya/Amu Darya, Uzboy, and the Caspian Sea. A more extensive glaciation during the penultimate (Dabudaer) glacial in the Himalaya/Pamir (Owen et al., 2012; Owen and Dortch, 2014; Hughes and Gibbard, 2018) would be in line with a contribution of high Sr-radiogenic

glacier meltwater from central Asia during the penultimate glacial and its absence during the last glacial in the Black Sea "Lake" (Major et al., 2006).

5.4 Penultimate glacial maximum and Termination II: 145-130 ka BP (MIS 6b-a)

Since ca. 148 ka BP, the northern summer insolation decreased to a minimum at ca. 138 ka BP (Fig. 6A; Berger and Loutre, 1991), which coincides with an expanded Eurasian Ice Sheet (Warthe ice advance) culminating during the penultimate glacial maximum at around 140 ka BP (Fig. 6C, Colleoni et al., 2016). Between 145 ka BP and 135 ka BP, temperatures seem to have fluctuated only slightly in the Greenland region (Barker et al., 2011). The T II–warming followed the increase of insolation and the final retreat of the Eurasian Sheet preluding the Eemian interglacial. In the North Atlantic/western Mediterranean region, warming took place already since ca. 142 ka BP, which was shortly interrupted by the Younger-Dryas-like cooling period between 131 ka BP and 129 ka BP (Fig. 6E, Martrat et al., 2004, 2007).

In the Black Sea region, temperatures remained at a low level and started to rise since ca. 131 ka BP as witnessed by increasing $Mg/Ca_{ostracods}$ ratios, slightly increasing surface temperatures, and decreasing IRD_C (Figs. 5E, 6F; Wegwerth et al., 2014 and this study). A Younger-Dryas-like cold period in the Black Sea remained questionable from a previous study (Shumilovskikh et al., 2013b; Wegwerth et al., 2014). Relatively low and constant TOC and TIC contents suggest persistence of the low productivity (Fig. 5F, G).

The $\delta^{18}O_{ostracod}$ record shows a long-term decline and fluctuations only on a low level (Fig. 6H). Two periods with a strong decrease of $\delta^{18}O_{ostracod}$ and lowered $Sr/Ca_{ostracods}$ imply two periods of meltwater discharge and freshening in the Black Sea "Lake" around 137 ka BP and 132 ka BP (Fig. 5A, C). The former corresponds to the aforementioned meltwater pulse BSWP-II (Wegwerth et al., 2014), whereas the first likely points to first indications of the ultimate collapse of the Eurasian Ice Sheet. Although not visible in the volume of the Eurasian Ice Sheet (Bintanja and van de Wal, 2008), an increasing global sea level already since ca. 139

836 ka BP (Grant et al., 2012) corroborates a retreat of the continental ice sheets and substantial
837 meltwater release shortly after the penultimate glacial maximum. Increasing sedimentary K/Ti
838 since ca. 139 ka BP suggests enhanced discharge from the northern and western rivers, in
839 agreement with the meltwater contribution.

840 Similar to BSWP-II (compare with chapter 5.3), higher radiogenic Sr-isotopes of the
841 ostracods at 137 ka BP (0.709043) likely point to a surplus of glacier water from the Tian Shan
842 and Pamir Mountains via the Caspian Sea (Fig. 6I). Although the Sofular Cave bears a gap
843 during that short period, faunal evidence from Black Sea sediments supports a Caspian-Black
844 Sea connection (Svitoch et al., 2000) already since 138 ka BP. During BSWP-II, $^{87}Sr/^{86}Sr_{ostracod}$
845 values increase to 0.709452 between 132 and 131 ka BP and represent the maximum of the
846 entire MIS 6 (Wegwerth et al., 2014, Fig. 6I).

847 The strongly increasing $Mg/Ca_{ostracod}$ values (Fig. 6F) reflect the warming during
848 Termination II and the Eemian, as discussed in detail by Wegwerth et al. (2014). The warming
849 was accompanied by the global sea-level rise (Grant et al., 2012) resulting in the Mediterranean-
850 Black Sea reconnection, an increased salinity of up to 30‰ (Shumilovskikh et al., 2013a), and
851 sapropel formation (Wegwerth et al., 2014, 2018). Shortly after the connection, the higher
852 $Sr/Ca_{ostracod}$ values point to increasing salinity, while the strongly increasing TOC contents
853 reflect the sapropel formation (Fig. 5C, G). Approximately 1 ka after the reconnection,
854 ostracods disappeared due to sulphidic bottom water conditions (Wegwerth et al., 2018).

855

856 **6. Summary and concluding remarks**

857 The present study provides a multi-proxy record from the former Black Sea "Lake"
858 covering almost the entire MIS 6 (184-130 ka BP). Warmer and more productive conditions
859 during the first (older) half of MIS 6 coincide with an insolation maximum and suggest
860 Dansgaard-Oeschger-like interstadials. The second (younger) half of MIS 6 shows a more
861 homogeneous picture with generally colder conditions and lower productivity.

The most remarkable finding of the present study results from the combination of $\delta^{18}O_{ostracod}$ and $^{87}Sr/^{86}Sr_{ostracod}$ records. The $\delta^{18}O_{ostracod}$ record demonstrates a strong response to the growing and shrinking Eurasian Ice Sheet fingerprinting meltwater release into the Black Sea "Lake". During periods of increased northern-hemispheric summer insolation, three main periods with pronounced and long-term negative excursions of $\delta^{18}O_{ostracod}$ indicate intense meltwater discharge with considerably higher amounts than during the last glacial. The marked dissimilarity in the $^{87}Sr/^{86}Sr_{ostracod}$ signatures between the meltwater periods during the first and second half of MIS 6 requires different meltwater pathways and sources.

The relatively low $^{87}Sr/^{86}Sr_{ostracod}$ values along with a dominance of Caspian ostracod species during the first meltwater period (180-167 ka BP) suggest a connection to the Caspian Sea and a freshwater source in the eastern Eurasian Ice Sheet. During the second and third meltwater periods, the Sr-isotopes of the ostracods are highly radiogenic. This can be explained either by a source in the radiogenic Precambrian craton of Scandinavia or by an origin in the Himalayan foothills, where loess and rivers carry a high Sr-radiogenic signature. However, since the Scandinavian craton was completely covered by the Eurasian Ice Sheet during that time, it is probably more conceivable that during the last two meltwater periods, a surplus of radiogenic water from glaciers in the Tian Shan and Pamir Mountains entered the Black Sea via the rivers Amu Darya, Syr Darya, and Uzboy, and the Caspian Sea. Future Sr-isotope analyses of rivers originating from the Tian Shan, Pamir, and Himalaya would support a better understanding of meltwater pathways and the dynamics of the palaeo-channel history in the Caspian-Aral Sea drainage basin. If our suggestion of an interplay between western Himalayan mountains and the Caspian/Black Sea region will be supported by future studies, the Himalayan region likely impacted the Caspian sea level not only during the Holocene (Leroy et al., 2007, 2013), but also during glacial times.

Concerning the extreme negative excursions in the $\delta^{18}O_{ostracod}$ record, that suggests pronounced contribution of meltwater, all three intervals were likely associated with lake level

rise and potentially with an overflow into the Marmara and Mediterranean Seas. Interestingly, the first and strongest meltwater period falls within the formation of the so-called "cold sapropel" S6 in the Mediterranean Sea (Bard et al., 2002; Schmiedl et al., 2003; Rohling et al., 2015). Although, the freshening in the Mediterranean Sea during S6 formation probably resulted mostly from high African monsoonal activity and freshwater discharge from the river Nile causing density stratification that favoured sapropel formation (Bard et al., 2002; Schmiedl et al., 2003; Rohling et al., 2015), a surplus from outflowing Black Sea "Lake" freshwater may have contributed as well.

Acknowledgements

The authors thank the captain and crew of RV Maria S. Merian for their support during the MSM33 Black Sea cruise in 2013. Technical/analytical support by Oona Appelt, Anne Köhler, Silja Kröger, Ina Neugebauer, Sylvia Pinkerneil, Sascha Plewe, Elmar Reitter, and Ines Scherff is greatly acknowledged. A.W. warmly thanks Lyudmila S. Shumilovskikh for palynological inspection of selected sediment samples. A.W. kindly thanks Gabriella Kolati for providing datasets of the Abaliget Cave speleothems and Anna Stepanova and Carlos Zarikian for support during ostracod identification. The authors thank three anonymous reviewers for constructive comments that improved the manuscript and A. Voelker for editorial handling. This work was funded through grant by DFG to A. Wegwerth (WE 6136/1-1; BlackPearl).

Data Availability

The data used in the present study are available online as supplementary data files at the Data Publisher for Earth and Environmental Science PANGAEA (http://www.pangaea.de).

References

Abe-Ouchi, A., Saito, F., Kawamura, K., Raymo, M.E., Okuno, J.i., Takahashi, K., Blatter, H., 2013. Insolation-driven 100,000-year glacial cycles and hysteresis of ice-sheet volume. Nature 500 (7461), 190-193. https://doi.org/10.1038/nature12374.

Aloisi, G., Soulet, G., Henry, P., Wallmann, K., Sauvestre, R., Vallet-Coulomb, C., Lécuyer, C., Bard, E., 2015. Freshening of the Marmara Sea prior to its post-glacial reconnection to the Mediterranean Sea. Earth Planet. Sci. Lett. 413, 176-185. https://doi.org/10.1016/j.epsl.2014.12.052.

Altherr, R., Topuz, G., Siebel, W., Şen, C., Meyer, H.-P., Satır, M., Lahaye, Y., 2008. Geochemical and Sr–Nd–Pb isotopic characteristics of Paleocene plagioleucitites from the Eastern Pontides (NE Turkey). Lithos 105, 149-161. http://dx.doi.org/10.1016/j.lithos.2008.03.001.

Ankindinova, O., Hiscott, R.N., Aksu, A.E., Grimes, V., 2019. High-resolution Sr-isotopic evolution of Black Sea water during the Holocene: Implications for reconnection with the global ocean. Mar. Geol. 407, 213-228. https://doi.org/10.1016/j.margeo.2018.11.004.

Arkhipov, S.A., Ehlers, J., Johnson, R.G., Wright, J.H.E., 1995. Glacial drainage towards the Mediterranean during the Middle and Late Pleistocene. Boreas 24, 196-206. https://doi.org/10.1111/j.1502-3885.1995.tb00773.x.

Arz, H.W., Böttcher, M., Burmeister, C., Dellwig, O., Fisch, K., Hehl, U., Jeschek, J., Jürgens, K., Kaiser, D., Konovalov, S.K., Krüger, S., Laudan, C., Lipka, M., Meeske, C., Melnikov, V., Olgun

Kiyak, N., Orekhova, N., Orlikowska, A., Plewe, S., Pollehne, F., Proskurnin, V., Scholz, C., Schuffenhauer, I., Schulz-Bull, D., Schulz-Vogt, H., Shumilovskikh, L., Wegwerth, A., Wlost, K.-P., 2014. Biological/biogeochemical processes and element fluxes at the Black Sea pelagic redoxcline, sedimentation processes and the late holocene development of the system - cruise MSM33 - November 2 - December 6, 2013 - Cádiz (Spain) - Varna (Bulgaria). MARIA MERIAN Berichte. http://dx.doi.org/10.2312/cr_msm33.

Ayalon, A., Bar-Matthews, M., Kaufman, A., 2002. Climatic conditions during marine oxygen isotope stage 6 in the eastern Mediterranean region from the isotopic composition of speleothems of Soreq Cave, Israel. Geology 30, 303-306. https://doi.org/10.1130/0091-7613(2002)030<0303:CCDMOI>2.0.CO;2.

Aydin, F., Karsli, O., Chen, B., 2008. Petrogenesis of the Neogene alkaline volcanics with implications for post-collisional lithospheric thinning of the Eastern Pontides, NE Turkey. Lithos 104, 249-266. http://dx.doi.org/10.1016/j.lithos.2007.12.010.

Bachmann, O., Schoene, B., Schnyder, C., Spikings, R., 2010. The 40Ar/39Ar and U/Pb dating of young rhyolites in the Kos-Nisyros volcanic complex, Eastern Aegean Arc, Greece: Age discordance due to excess 40Ar in biotite. Geochem. Geophys. Geosyst. 11. Q0AA08 https://doi.org/10.1029/2010GC003073.

Badertscher, S., Fleitmann, D., Cheng, H., Edwards, R.L., Gokturk, O.M., Zumbuhl, A., Leuenberger, M., Tuysuz, O., 2011. Pleistocene water intrusions from the Mediterranean and Caspian seas into the Black Sea. Nat. Geosci. 4 (4), 236-239. http://dx.doi.org/10.1038/ngeo1106.

Bahr, A., Arz, H.W., Lamy, F., Wefer, G., 2006. Late glacial to Holocene paleoenvironmental evolution of the Black Sea, reconstructed with stable oxygen isotope records obtained on ostracod shells. Earth Planet. Sci. Lett. 241, 863-875. https://doi.org/10.1016/j.epsl.2005.10.036.

Bahr, A., Lamy, F., Arz, H.W., Major, C., Kwiecien, O., Wefer, G., 2008. Abrupt changes of temperature and water chemistry in the late Pleistocene and early Holocene Black Sea. Geochem. Geophys. Geosyst. 9, Q01004. http://dx.doi.org/10.1029/2007GC001683.

Bard, E., Delaygue, G., Rostek, F., Antonioli, F., Silenzi, S., Schrag, D.P., 2002. Hydrological conditions over the western Mediterranean basin during the deposition of the cold Sapropel 6 (ca. 175 kyr BP). Earth Planet. Sci. Lett. 202, 481-494. https://doi.org/10.1016/S0012-821X(02)00788-4.

Barker, S., Knorr, G., Edwards, R.L., Parrenin, F., Putnam, A.E., Skinner, L.C., Wolff, E., Ziegler, M., 2011. 800,000 Years of Abrupt Climate Variability. Science 334, 347-351. DOI: 10.1126/science.1203580.

Berger, A., Loutre, M.F., 1991. Insolation values for the climate of the last 10 million years. Quat. Sci. Rev. 10, 297-317. https://doi.org/10.1016/0277-3791(91)90033-Q.

Bintanja, R., van de Wal, R.S.W., 2008. North American ice-sheet dynamics and the onset of 100,000-year glacial cycles. Nature 454, 869-872. http://dx.doi.org/10.1038/nature07158.

Boomer, I., Aladin, N., Plotnikov, I., Whatley, R., 2000. The palaeolimnology of the Aral Sea: a review. Quat. Sci. Rev. 19, 1259-1278. https://doi.org/10.1016/S0277-3791(00)00002-0.

Boomer, I., von Grafenstein, U., Guichard, F., Bieda, S., 2005. Modern and Holocene sublittoral ostracod assemblages (Crustacea) from the Caspian Sea: A unique brackish, deep-water environment. Palaeogeogr. Palaeoclimatol. Palaeoecol. 225, 173-186. http://dx.doi.org/10.1016/j.palaeo.2004.10.023.

Boomer, I., Guichard, F., Lericolais, G., 2010. Late Pleistocene to Recent ostracod assemblages from the western Black Sea. J. Micropalaeontol. 29, 119e133. http://dx.doi.org/10.1144/0262-821X10-003.

Boomer, I., 2012. Chapter 12 - Ostracoda as Indicators of Climatic and Human-Influenced Changes in the Late Quaternary of the Ponto-Caspian Region (Aral, Caspian and Black Seas), in: Horne, D.J., Holmes, J.A., Rodriguez-Lazaro, J., Viehberg, F.A. (Eds.), Developments in Quaternary Sciences. Elsevier, pp. 205-215. http://dx.doi.org/10.1016/B978-0-444-53636-5.00012-3.

Boswell, S.M., Toucanne, S., Pitel-Roudaut, M., Creyts, T.T., Eynaud, F., Bayon, G., 2019. Enhanced surface melting of the Fennoscandian Ice Sheet during periods of North Atlantic cooling. Geology. https://doi.org/10.1130/G46370.1

Bourne, A.J., Albert, P.G., Matthews, I.P., Trincardi, F., Wulf, S., Asioli, A., Blockley, S.P.E., Keller, J. and Lowe, J.J. 2015. Tephrochronology of core PRAD 1-2 from the Adriatic Sea: insights into Italian explosive volcanism for the period 200-80 ka. Quat. Sci. Rev. 116, 28-43. https://doi.org/10.1016/j.quascirev.2015.03.006.

Burr, G.S., Kuzmin, Y.V., Krivonogov, S.K., Gusskov, S.A., Cruz, R.J., 2019. A history of the modern Aral Sea (Central Asia) since the Late Pleistocene. Quat. Sci. Rev. 206, 141-149. https://doi.org/10.1016/j.quascirev.2019.01.006.

Çağatay, M.N., Eriş, K., Ryan, W.B.F., Sancar, Ü., Polonia, A., Akçer, S., Biltekin, D., Gasperini, L., Görür, N., Lericolais, G., Bard, E., 2009. Late Pleistocene–Holocene evolution of the northern shelf of the Sea of Marmara. Mar. Geol. 265, 87-100. https://doi.org/10.1016/j.margeo.2009.06.011.

Çağatay, M.N., Öğretmen, N., Damcı, E., Stockhecke, M., Sancar, Ü., Eriş, K.K., Özeren, S., 2014. Lake level and climate records of the last 90 ka from the Northern Basin of Lake Van, eastern Turkey. Quaternary Science Reviews 104, 97-116. http://dx.doi.org/10.1016/j.quascirev.2014.09.027

Çağatay, M.N., Wulf, S., Sancar, Ü., Özmaral, A., Vidal, L., Henry, P., Appelt, O., Gasperini, L., 2015. The tephra record from the Sea of Marmara for the last ca. 70 ka and its palaeoceanographic implications. Marine Geology 361, 96-110. http://dx.doi.org/10.1016/j.margeo.2015.01.005.

Chepalyga, A.L., 2007. The late glacial great flood in the Ponto-Caspian basin, in: Yanko-Hombach, V., Gilbert, A.S., Panin, N., Dolukhanov, P.M. (Eds.), The Black Sea Flood Question: Changes in Coastline, Climate, and Human Settlement. Springer Netherlands, Dordrecht, pp. 119-148. https://doi.org/10.1007/978-1-4020-5302-3_6

Chivas, A.R., Deckker, P., Shelley, J.M.G., 1986. Magnesium and strontium in non-marine ostracod shells as indicators of palaeosalinity and palaeotemperature. Hydrobiologia 143, 135-142. http://dx.doi.org/10.1007/BF00026656.

Clauer, N., S. Chaudhuri, T. Toulkeridis, G. Blanc; Fluctuations of Caspian Sea level: Beyond climatic variations?. Geology ; 28 (11): 1015–1018. doi: https://doi.org/10.1130/0091-7613(2000)28<1015:FOCSLB>2.0.CO;2

Colleoni, F., Krinner, G., Jakobsson, M., Peyaud, V., Ritz, C., 2009. Influence of regional parameters on the surface mass balance of the Eurasian ice sheet during the peak Saalian (140 kya). Glob. Planet. Change 68, 132-148. https://doi.org/10.1016/j.gloplacha.2009.03.021.

Colleoni, F., Wekerle, C., Näslund, J.-O., Brandefelt, J., Masina, S., 2016. Constraint on the penultimate glacial maximum Northern Hemisphere ice topography (≈140 kyrs BP). Quat. Sci. Rev. 137, 97-112. http://dx.doi.org/10.1016/j.quascirev.2016.01.024.

Cox, J.M., Faure, G., 1974. Isotope composition of strontium in carbonate phase of two cores from Black Sea. In: Degens, E.T., Ross, D.A. (Eds.), The Black Sea—Geology, Chemistry and Biology. American Association of Petroleum Geologists, Tulsa, OK, pp. 566–569. https://doi.org/10.1306/M20377C19.

Cullen, H.M., deMenocal, P.B., 2000. North Atlantic influence on Tigris–Euphrates streamflow. International Journal of Climatology 20, 853-863. https://doi.org/10.1002/1097-0088(20000630)20:8<853::AID-JOC497>3.0.CO;2-M.

Dansgaard, W., Johnsen, S.J., Clausen, H.B., Dahl-Jensen, D., Gundestrup, N.S., Hammer, C.U., Hvidberg, C.S., Steffensen, J.P., Sveinbjornsdottir, A.E., Jouzel, J., Bond, G., 1993. Evidence for general instability of past climate from a 250-kyr ice-core record. Nature 364, 218-220. http://dx.doi.org/10.1038/364218a0.

Dellwig, O., Leipe, T., März, C., Glockzin, M., Pollehne, F., Schnetger, B., Yakushev, E.V., Böttcher, M.E., Brumsack, H.-J.r., 2010. A new particulate Mn-Fe-P-shuttle at the redoxcline of anoxic basins. Geochim. Cosmochim. Acta 74, 7100-7115. https://doi.org/10.1016/j.gca.2010.09.017.

Dellwig, O., Wegwerth, A., Schnetger, B., Schulz, H., Arz, H.W., 2019. Dissimilar behaviors of the geochemical twins W and Mo in hypoxic-euxinic marine basins. Earth Sci. Rev. 193, 1-23. https://doi.org/10.1016/j.earscirev.2019.03.017.

Demaison, G.J., Moore, G.T., 1980. Anoxic environments and oil source bed genesis. Org. Geochem. 2, 9-31. https://doi.org/10.1016/0146-6380(80)90017-0.

Deniz, A., Toros, H., Incecik, S., 2011. Spatial variations of climate indices in Turkey. Int. J. Climatol. 31, 394e403. http://dx.doi.org/10.1002/joc.2081.

Ehlers, J., Gibbard, P.L., 2007. The extent and chronology of Cenozoic Global Glaciation. Quat. Int. 164-165, 6-20. https://doi.org/10.1016/j.quaint.2006.10.008.

Ehlers, J., Grube, A., Stephan, H.-J., Wansa, S., 2011. Chapter 13 - Pleistocene Glaciations of North Germany—New Results, in: Ehlers, J., Gibbard, P.L., Hughes, P.D. (Eds.), Developments in Quaternary Sciences. Elsevier, pp. 149-162. doi: 10.1016/B978-0-444-53447-7.00013-1.

Engstrom, D.R., Nelson, S.R., 1991. Paleosalinity from trace metals in fossil ostracodes compared with observational records at Devils Lake, North Dakota, USA. Palaeogeogr. Palaeoclimatol. Palaeoecol. 83, 295e312. http://dx.doi.org/10.1016/0031-0182(91)90057-X.

Epstein, S., Buchsbaum, R., Lowenstam, H.A., Urey, H.C., 1953. Revised Carbonate-Water Isotopic Temperature Scale. GSA Bulletin 64, 1315-1326. 10.1130/0016-7606(1953)64[1315:rcits]2.0.co;2.

Federman, A. N. and Carey, S. N. 1980. Electron microprobe correlation of tephra layers from Eastern Mediterranean abyssal sediments and the island of Santorini. Quat. Res. 13, 160-171. https://doi.org/10.1016/0033-5894(80)90026-5.

Fleitmann, D., Cheng, H., Badertscher, S., Edwards, R.L., Mudelsee, M., Göktürk, O.M., Fankhauser, A., Pickering, R., Raible, C.C., Matter, A., Kramers, J., Tüysüz, O., 2009. Timing and climatic impact of Greenland interstadials recorded in stalagmites from northern Turkey. Geophys. Res. Lett. 36 (19), L19707. http://dx.doi.org/10.1029/2009GL040050.

Francke, A., Wagner, B., Just, J., Leicher, N., Gromig, R., Baumgarten, H., Vogel, H., Lacey, J.H., Sadori, L., Wonik, T., Leng, M.J., Zanchetta, G., Sulpizio, R., Giaccio, B., 2016. Sedimentological processes and environmental variability at Lake Ohrid (Macedonia, Albania) between 637 ka and the present. Biogeosciences 13, 1179-1196. https://doi.org/10.5194/bg-13-1179-2016

Giaccio, B., Niespolo, E.M., Pereira, A., Nomade, S., Renne, P. R., Albert, P. G., Arienzo, I., Regattieri, E., Wagner, B., Zanchetta, G., Gaeta, M., Galli, P., Mannella, G., Peronace, E., Sottili, G., Florindo, F., Leicher, N., Marra, F. and Tomlinson, E.L. 2017. First integrated tephrochronological record for the last ~ 190 kyr from the Fucino Quaternary lacustrine succession, central Italy. Quat. Sci. Rev. 158, 211-234. https://doi.org/10.1016/j.quascirev.2017.01.004.

Göktürk, O.M., Fleitmann, D., Badertscher, S., Cheng, H., Edwards, R.L., Leuenberger, M., Fankhauser, A., Tüysüz, O., Kramers, J., 2011. Climate on the southern Black Sea coast during the Holocene: implications from the Sofular Cave record. Quat. Sci. Rev. 30, 2433-2445. http://dx.doi.org/10.1016/j.quascirev.2011.05.007.

Grant, K.M., Rohling, E.J., Bar-Matthews, M., Ayalon, A., Medina-Elizalde, M., Ramsey, C.B., Satow, C., Roberts, A.P., 2012. Rapid coupling between ice volume and polar temperature over the past 150,000 years. Nature 491, 744-747. https://doi.org/10.1038/nature11593.

Grant, K.M., Rohling, E.J., Ramsey, C.B., Cheng, H., Edwards, R.L., Florindo, F., Heslop, D., Marra, F., Roberts, A.P., Tamisiea, M.E., Williams, F., 2014. Sea-level variability over five glacial cycles. Nat. Comm. 5. https://doi.org/10.1038/ncomms6076.

Heinrich, H., 1988. Origin and consequences of cyclic ice rafting in the Northeast Atlantic Ocean during the past 130,000 years. Quat. Res. 29 (2), 142e152. http://dx.doi.org/10.1016/0033-5894(88)90057-9.

Heinrichs, H., Brumsack, H.-J., Loftfield, N., König, N., 1986. Verbessertes Druckaufschlußsystem für biologische und anorganische Materialien. Z. Pflanzenernähr. Bodenkd. 149, 350–353. http://dx.doi.org/10.1002/jpln.19861490313.

Henderson, G.M., Martel, D.J., O'Nions, R.K., Shackleton, N.J., 1994. Evolution of seawater 87Sr86Sr over the last 400 ka: the absence of glacial/interglacial cycles. Earth Planet. Sci. Lett. 128, 643-651. https://doi.org/10.1016/0012-821X(94)90176-7.

Hughes, A.L.C., Gyllencreutz, R., Lohne, Ø.S., Mangerud, J., Svendsen, J.I., 2016. The last Eurasian ice sheets – a chronological database and time-slice reconstruction, DATED-1. Boreas 45, 1-45. https://doi.org/10.1111/bor.12142.

Hughes, P.D., Gibbard, P.L., 2018. Global glacier dynamics during 100 ka Pleistocene glacial cycles. Quat. Res. 90, 222-243. https://doi.org/10.1017/qua.2018.37.

Hunt, J.B., Hill, P.G., 1996. An inter-laboratory comparison of the electron probe microanalysis of glass geochemistry. Quat. Int. 34-36, 229-241. https://doi.org/10.1016/1040-6182(95)00088-7.

Imbrie, J., McIntyre, A., Mix, A., 1989. Oceanic Response to Orbital Forcing in the Late Quaternary: Observational and Experimental Strategies, in: Berger, A., Schneider, S., Duplessy, J.C. (Eds.), Climate and Geo-Sciences: A Challenge for Science and Society in the 21st Century. Springer Netherlands, Dordrecht, pp. 121-164. https://doi.org/10.1007/978-94-009-2446-8_7.

Jacobson, A.D., Blum, J.D., Walter, L.M., 2002. Reconciling the elemental and Sr isotope composition of Himalayan weathering fluxes: insights from the carbonate geochemistry of stream waters. Geochim. Cosmochim. Acta 66, 3417-3429. https://doi.org/10.1016/S0016-7037(02)00951-1.

Janz, H., Vennemann, T.W., 2005. Isotopic composition (O, C, Sr, and Nd) and trace element ratios (Sr / Ca, Mg / Ca) of Miocene marine and brackish ostracods from North Alpine Foreland deposits

(Germany and Austria) as indicators for palaeoclimate. Palaeogeogr. Palaeoclimatol. Palaeoecol. 225, 216-247. https://doi.org/10.1016/j.palaeo.2005.06.012.

Jochum, K.P., Stoll, B., Herwig, K., Willbold, M., Hofmann, A.W., Amini, M., Aarburg, S. et al. 2006. MPI-DING reference glasses for in situ microanalysis: New reference values for element concentrations and isotope ratios. Geochem. Geophys. Geosyst. 7, Q02008. https://doi.org/10.1029/2005GC001060.

Kaygusuz, A., Aydınçakır, E., 2009. Mineralogy, whole-rock and Sr–Nd isotope geochemistry of mafic microgranular enclaves in Cretaceous Dagbasi granitoids, Eastern Pontides, NE Turkey: Evidence of magma mixing, mingling and chemical equilibration. Chemie der Erde - Geochemistry 69, 247-277. http://dx.doi.org/10.1016/j.chemer.2008.08.002.

Kern, Z.; Demény, A..; Hatvani, I.G. Speleothem Stable Isotope Records from Eastern Europe & Turkey. Preprints 2018, 2018120038, doi: 10.20944/preprints201812.0038.v1.

Koltai, G., Spötl, C., Shen, C.C., Wu, C.C., Rao, Z., Palcsu, L., Kele, S., Surányi, G., Bárány-Kevei, I., 2017. A penultimate glacial climate record from southern Hungary. J. Quat. Sci. 32, 946-956. https://doi.org/10.1002/jqs.2968.

Kuehn, S.C., Froese, D.G., Shane, P.A.R., 2011. The INTAV intercomparison of electron-beam microanalysis of glass by tephrochronology laboratories: Results and recommendations. Quat. Int. 246, 19-47. https://doi.org/10.1016/j.quaint.2011.08.022.

Lachniet, M.S., 2009. Climatic and environmental controls on speleothem oxygen-isotope values. Quat. Sci. Rev. 28, 412-432. https://doi.org/10.1016/j.quascirev.2008.10.021.

Lambeck, K., 1996. Limits on the areal extent of the Barents Sea ice sheet in Late Weichselian time. Glob. Planet. Change 12, 41-51. https://doi.org/10.1016/0921-8181(95)00011-9.

Lambeck, K., Purcell, A., Funder, S., Kjær, K.H., Larsen, E., Moller, P., 2006. Constraints on the Late Saalian to early Middle Weichselian ice sheet of Eurasia from field data and rebound modelling. Boreas 35, 539-575. https://doi.org/10.1080/03009480600781875.

Lamy, F., Arz, H.W., Bond, G.C., Bahr, A., Pätzold, J., 2006. Multicentennial-scale hydrological changes in the Black Sea and northern Red Sea during the Holocene and the Arctic/North Atlantic Oscillation. Paleoceanography 21, PA1008. http://dx.doi.org/10.1029/2005PA001184.

Lang, J., Lauer, T., Winsemann, J., 2018. New age constraints for the Saalian glaciation in northern central Europe: Implications for the extent of ice sheets and related proglacial lake systems. Quat. Sci. Rev. 180, 240-259. https://doi.org/10.1016/j.quascirev.2017.11.029.

Larsen, E., KjæR, K.H., Demidov, I.N., Funder, S., Grøsfjeld, K., Houmark-Nielsen, M., Jensen, M., Linge, H., Lysa, A., 2006. Late Pleistocene glacial and lake history of northwestern Russia. Boreas 35, 394-424. https://doi.org/10.1080/03009480600781958.

Laskar, J., Robutel, P., Joutel, F., Gastineau, M., Correia, A.C.M., Levrard, B., 2004. A long-term numerical solution for the insolation quantities of the Earth. A&A 428, 261-285. https://doi.org/10.1051/0004-6361:20041335.

Lebedev, V.A., Bubnov, S.N., Chernyshev, I.V., Chugaev, A.V., Dudauri, O.Z., Vashakidze, G.T., 2007. Geochronology and genesis of subalkaline basaltic lava rivers at the Dzhavakheti highland, lesser Caucasus: K-Ar and Sr-Nd isotopic data. Geochem. Int. 45, 211-225. https://doi.org/10.1134/S0016702907030019.

Leicher, N., Zanchetta, G., Sulpizio, R., Giaccio, B., Wagner, B., Nomade, S., Francke, A. and Del Carlo, P. 2016. First tephrostratigraphic results of the DEEP site record from Lake Ohrid (Macedonia and Albania). Biogeosciences 13, 2151-2178. https://doi.org/10.5194/bg-13-2151-2016.

Leroy, S.A.G., Arpe, K., 2007. Glacial refugia for summer-green trees in Europe and south-west Asia as proposed by ECHAM3 time-slice atmospheric model simulations. J. Biogeogr. 34, 2115-2128. https://doi.org/10.1111/j.1365-2699.2007.01754.x

Leroy, S.A.G., Kakroodi, A.A., Kroonenberg, S., Lahijani, H.K., Alimohammadian, H., Nigarov, A., 2013. Holocene vegetation history and sea level changes in the SE corner of the Caspian Sea: relevance to SW Asia climate. Quat. Sci. Rev. 70, 28-47. https://doi.org/10.1016/j.quascirev.2013.03.004.

Lisiecki, L.E., Raymo, M.E., 2005. A Pliocene-Pleistocene stack of 57 globally distributed benthic $\delta^{18}O$ records. Paleoceanography 20. doi:10.1029/2004PA001071.

Lototskaya, A., Ganssen, G.M., 1999. The structure of Termination II (penultimate deglaciation and Eemian) in the North Atlantic. Quat. Sci. Rev. 18, 1641-1654. https://doi.org/10.1016/S0277-3791(99)00011-6.

Major, C.O., Goldstein, S.L., Ryan, W.B.F., Lericolais, G., Piotrowski, A.M., Hajdas, I., 2006. The co-evolution of Black Sea level and composition through the last deglaciation and its paleoclimatic significance. Quat. Sci. Rev. 25, 2031-2047. https://doi.org/10.1016/j.quascirev.2006.01.032.

Margari, V., Skinner, L.C., Tzedakis, P.C., Ganopolski, A., Vautravers, M., Shackleton, N.J., 2010. The nature of millennial-scale climate variability during the past two glacial periods. Nat. Geosci. 3, 127-131. https://doi.org/10.1038/ngeo740.

Margari, V., Skinner, L.C., Hodell, D.A., Martrat, B., Toucanne, S., Grimalt, J.O., Gibbard, P.L., Lunkka, J.P., Tzedakis, P.C., 2014. Land-ocean changes on orbital and millennial time scales and the penultimate glaciation. Geology 42, 183-186. https://doi.org/10.1130/G35070.1.

Marks, L., Karabanov, A., Nitychoruk, J., Bahdasarau, M., Krzywicki, T., Majecka, A., Pochocka-Szwarc, K., Rychel, J., Woronko, B., Zbucki, Ł., Hradunova, A., Hrychanik, M., Mamchyk, S., Rylova, T., Nowacki, Ł., Pielach, M., 2018. Revised limit of the Saalian ice sheet in central Europe. Quat. Int. 478, 59-74. https://doi.org/10.1016/j.quaint.2016.07.043.

Marret, F., Leroy, S., Chalié, F., Françoise, F., 2004. New organic-walled dinoflagellate cysts from recent sediments of Central Asian seas. Review of Palaeobotany and Palynology 129, 1-20. https://doi.org/10.1016/j.revpalbo.2003.10.002

Martrat, B., Grimalt, J.O., Lopez-Martinez, C., Cacho, I., Sierro, F.J., Flores, J.A., Zahn, R., Canals, M., Curtis, J.H., Hodell, D.A., 2004. Abrupt Temperature Changes in the Western Mediterranean over the Past 250,000 Years. Science 306, 1762-1765. DOI: 10.1126/science.1101706.

Martrat, B., Grimalt, J.O., Shackleton, N.J., de Abreu, L., Hutterli, M.A., Stocker, T.F., 2007. Four Climate Cycles of Recurring Deep and Surface Water Destabilizations on the Iberian Margin. Science 317, 502-507. DOI: 10.1126/science.1139994.

McCrea, J.M., 1950. On the Isotopic Chemistry of Carbonates and a Paleotemperature Scale. The Journal of Chemical Physics 18, 849-857. https://doi.org/10.1063/1.1747785.

Meknassi, S. El, G. Dera, T. Cardone, M. De Rafélis, C. Brahmi, V. Chavagnac, 2018. Sr isotope ratios of modern carbonate shells: Good and bad news for chemostratigraphy. Geology ; 46 (11): 1003–1006. doi: https://doi.org/10.1130/G45380.1

Mengel, K., Borsuk, A.M., Gurbanov, A.G., Wedepohl, K.H., Baumann, A., Hoefs, J., 1987. Origin of spilitic rocks from the southern slope of the Greater Caucasus. Lithos 20, 115-133. http://dx.doi.org/10.1016/0024-4937(87)90002-8.

Menviel, L., Capron, E., Govin, A., Dutton, A., Tarasov, L., Abe-Ouchi, A., Drysdale, R., Gibbard, P., Gregoire, L., He, F., Ivanovic, R., Kageyama, M., Kawamura, K., Landais, A., Otto-Bliesner, B.L., Oyabu, I., Tzedakis, P., Wolff, E., Zhang, X., 2018. The penultimate deglaciation: protocol for PMIP4 transient numerical simulations between 140 and 127 ka. Clim. Past Discuss. 2018, 1-53. https://doi.org/10.5194/cp-2018-106

Milanković, M., 1969. Canon of insolation and the ice-age problem: (Kanon der Erdbestrahlung und seine Anwendung auf das Eiszeitenproblem) Belgrade, 1941. Israel Program for Scientific Translations; [available from U.S. Dept. of Commerce, Clearinghouse for Federal Scientific and Technical Information, Springfield, Va.].

Murray, J., 1900. On the deposits of the black sea. Scott. Geogr. Mag. 16, 673-702. http://dx.doi.org/10.1080/00369220008733207.

Murray, J.W., Stewart, K., Kassakian, S., Krynytzky, M., DiJulio, D., 2007. Oxic, suboxic, and anoxic conditions in the Black Sea. In The Black Sea Flood Question (eds. V. Yanko-Hombach, A. S. Gilbert, N. Panin and P. M. Dolukhaov).Springer, Dordrecht, pp. 1–21. https://doi.org/10.1007/978-1-4020-5302-3_1

Négrel, P., Casanova, J., Blomqvist, R., 2005. 87Sr/86Sr of brines from the Fennoscandian Shield: a synthesis of groundwater isotopic data from the Baltic Sea region. Can. J. Earth Sci. 42, 273-285. doi: 10.1139/E04-103.

Nezlin, N., 2006. Seasonal and Interannual Variability of Remotely Sensed Chlorophyll, in: Kostianoy, A., Kosarev, A. (Eds.), The Black Sea Environment. Springer Berlin Heidelberg, pp. 333-349. https://doi.org/10.1007/698_5_063.

Nowaczyk, N.R., Arz, H.W., Frank, U., Kind, J., Plessen, B., 2012. Dynamics of the Laschamp geomagnetic excursion from Black Sea sediments. Earth Planet. Sci. Lett. 351-352, 54-69. http://dx.doi.org/10.1016/j.epsl.2012.06.050.

Obrochta, S.P., Crowley, T.J., Channell, J.E.T., Hodell, D.A., Baker, P.A., Seki, A., Yokoyama, Y., 2014. Climate variability and ice-sheet dynamics during the last three glaciations. Earth Planet. Sci. Lett. 406, 198-212. http://dx.doi.org/10.1016/j.epsl.2014.09.004.

1213 Olteanu, R., 1978. Ostracoda from DSDP Leg 42B. Affiliation (analytic): Inst. Oceanogr. Sci., Wormley
1214 42, 1017. doi: 10.2973/dsdp.proc.42-2.145.1978.
1215 Owen, L.A., Chen, J., Hedrick, K.A., Caffee, M.W., Robinson, A.C., Schoenbohm, L.M., Yuan, Z., Li,
1216 W., Imrecke, D.B., Liu, J., 2012. Quaternary glaciation of the Tashkurgan Valley, Southeast Pamir.
1217 Quat. Sci. Rev. 47, 56-72. https://doi.org/10.1016/j.quascirev.2012.04.027.
1218 Owen, L.A., Dortch, J.M., 2014. Nature and timing of Quaternary glaciation in the Himalayan–Tibetan
1219 orogen. Quat. Sci. Rev. 88, 14-54. https://doi.org/10.1016/j.quascirev.2013.11.016.
1220 Özsoy, E., Ünlüata, Ü., 1997. Oceanography of the Black Sea: A review of some recent results. Earth
1221 Sci. Rev. 42, 231-272. http://dx.doi.org/10.1016/S0012-8252(97) 81859-4.
1222 Özsoy, E., Rank, D., Salihoglu, I., 2002. Pycnocline and Deep Mixing in the Black Sea: Stable Isotope
1223 and Transient Tracer Measurements. Estuar. Coast. Shelf Sci. 54, 621-629.
1224 https://doi.org/10.1006/ecss.2000.0669.
1225 Page, A., Vance, D., Fowler, M., Nisbet, E., 2003. Modern Sr isotopic mass balance and Quaternary
1226 variation in the Caspian Sea. EGS - AGU - EUG Joint Assembly, Abstracts from the meeting held
1227 in Nice, France, 6 - 11 April 2003, abstract #3242.
1228 Palmer, M.R., Edmond, J.M., 1989. The strontium isotope budget of the modern ocean. Earth Planet.
1229 Sci. Lett. 92, 11-26. https://doi.org/10.1016/0012-821X(89)90017-4.
1230 Paterne, M., Guichard, F., Duplessy, J.C., Siani, G., Sulpizio, R., Labeyrie, J., 2008. A 90,000-200,000
1231 yrs marine tephra record of Italian volcanic activity in the Central Mediterranean Sea. J. Volcanol.
1232 Geoth. Res. 177, 187-196. https://doi.org/10.1016/j.jvolgeores.2007.11.028.
1233 Penaud, A., Eynaud, F., Turon, J.L., Zaragosi, S., Malaizé, B., Toucanne, S., Bourillet, J.F., 2009. What
1234 forced the collapse of European ice sheets during the last two glacial periods (150 ka B.P. and 18
1235 ka cal B.P.)? Palynological evidence. Palaeogeogr. Palaeoclimatol. Palaeoecol. 281, 66-78.
1236 http://dx.doi.org/10.1016/j.palaeo.2009.07.012.
1237 Piper, D.Z., Calvert, S.E., 2011. Holocene and late glacial palaeoceanography and palaeolimnology of
1238 the Black Sea: Changing sediment provenance and basin hydrography over the past 20,000 years.
1239 Geochim. Cosmochim. Acta 75, 5597-5624. http://dx.doi.org/10.1016/j.gca.2011.07.016.
1240 Piva, A., Asioli, A., Andersen, N., Grimalt, J.O., Schneider, R.R., Trincardi, F., 2008. Climatic cycles
1241 as expressed in sediments of the PROMESS1 borehole PRAD1-2, central Adriatic, for the last 370
1242 ka: 2. Paleoenvironmental evolution. Geochemistry, Geophysics, Geosystems 9, Q03R02.
1243 https://doi.org/10.1029/2007GC001785.
1244 Pokrovsky, B.G., Zaviyalov, P.O., Bujakaite, M.I., Izhitskiy, A.S., Petrov, O.L., Kurbaniyazov, A.K.,
1245 Shimanovich, V.M., 2017. Geochemistry of O, H, C, S, and Sr isotopes in the water and sediments
1246 of the Aral basin. Geochem. Int. 55, 1033-1045. https://doi.org/10.1134/S0016702917110076.
1247 Quan, T.M., Wright, J.D., Falkowski, P.G., 2013. Co-variation of nitrogen isotopes and redox states
1248 through glacial-interglacial cycles in the Black Sea. Geochim. Cosmochim. Acta 112, 305-320.
1249 http://dx.doi.org/10.1016/j.gca.2013.02.029.
1250 Railsback, L.B., Gibbard, P.L., Head, M.J., Voarintsoa, N.R.G., Toucanne, S., 2015. An optimized
1251 scheme of lettered marine isotope substages for the last 1.0 million years, and the
1252 climatostratigraphic nature of isotope stages and substages. Quat. Sci. Rev. 111, 94-106.
1253 https://doi.org/10.1016/j.quascirev.2015.01.012.
1254 Regattieri, E., Zanchetta, G., Drysdale, R.N., Isola, I., Hellstrom, J.C., Roncioni, A., 2014. A continuous
1255 stable isotope record from the penultimate glacial maximum to the Last Interglacial (159–121ka)
1256 from Tana Che Urla Cave (Apuan Alps, central Italy). Quat. Res. 82, 450-461.
1257 https://doi.org/10.1016/j.yqres.2014.05.005.
1258 Reinhardt, E.G., Blenkinsop, J., Patterson, R.T., 1998. Assessment of a Sr isotope vital effect
1259 (87Sr/86Sr) in marine taxa from Lee Stocking Island, Bahamas. Geo-Mar. Lett. 18, 241-246.
1260 https://doi.org/10.1007/s003670050074.
1261 Repeta, D.J., Simpson, D.J., Jorgensen, B.B., Jannasch, H.W., 1989. Evidence for anoxygenic
1262 photosynthesis from the distribution of bacterio-chlorophylls in the Black Sea. Nature 342, 69-72.
1263 http://dx.doi.org/10.1038/342069a0.
1264 Richards, K., Mudie, P., Rochon, A., Athersuch, J., Bolikhovskaya, N., Hoogendoorn, R., Verlinden,
1265 V., 2017. Late Pleistocene to Holocene evolution of the Emba Delta, Kazakhstan, and coastline of
1266 the north-eastern Caspian Sea: Sediment, ostracods, pollen and dinoflagellate cyst records.
1267 Palaeogeogr. Palaeoclimatol. Palaeoecol. 468, 427-452.
1268 https://doi.org/10.1016/j.palaeo.2016.12.035.

Rohling, E.J., Marino, G., Grant, K.M., 2015. Mediterranean climate and oceanography, and the periodic development of anoxic events (sapropels). Earth-Sci. Rev. 143, 62-97. http://dx.doi.org/10.1016/j.earscirev.2015.01.008.

Rotolo, S. G., Scaillet, S., La Felice, S., Vita-Scaillet, G., 2013. A revision of the structure and stratigraphy of pre-Green Tuff ingimbrites at Pantelleria (Strait of Sicily), J. Volcanol. Geoth. Res. 250, 61–74. https://doi.org/10.1016/j.jvolgeores.2012.10.009.

Sarnthein, M., Tiedemann, R., 1990. Younger Dryas-Style Cooling Events at Glacial Terminations I-VI at ODP Site 658: Associated benthic δ13C anomalies constrain meltwater hypothesis. Paleoceanography 5, 1041-1055. https://doi.org/10.1029/PA005i006p01041.

Satow, C., Tomlinson, E. L., Grant, K. M., Albert, P. G., Smith, V. C., Manning, C. J., Ottolini, L., Wulf, S., Rohling, E.J., Lowe, J.J., Blockley, S.P.E. and Menzies, M. A. 2015. A new contribution to the Late Quaternary tephrostratigraphy of the Mediterranean: Aegean Sea core LC21. Quat. Sci. Rev. 117, 96-112. https://doi.org/10.1016/j.quascirev.2015.04.005.

Schmiedl, G., Mitschele, A., Beck, S., Emeis, K.-C., Hemleben, C., Schulz, H., Sperling, M., Weldeab, S., 2003. Benthic foraminiferal record of ecosystem variability in the eastern Mediterranean Sea during times of sapropel S5 and S6 deposition. Palaeogeogr. Palaeoclimatol. Palaeoecol. 190, 139-164. https://doi.org/10.1016/S0031-0182(02)00603-X.

Schmincke, H.-U., Sumita, M. and team, P. s. 2014. Impact of volcanism on the evolution of Lake Van (eastern Anatolia) III: Periodic (Nemrut) vs. episodic (Süphan) explosive eruptions and climate forcing reflected in a tephra gap between ca. 14 ka and ca. 30 ka. J. Volcanol. Geoth. Res. 285, 195-213. https://doi.org/10.1016/j.jvolgeores.2014.08.015.

Schmitt, A.K., Danišík, M., Evans, N.J., Siebel, W., Kiemele, E., Aydin, F., Harvey, J.C., 2011. Acigöl rhyolite field, Central Anatolia (part 1): high-resolution dating of eruption episodes and zircon growth rates. Contrib. Mineral. Petrol. 162, 1215-1231. https://doi.org/10.1007.

Schnetger, B., 1997. Trace element analysis of sediments by HR-ICP-MS using low and medium resolution and different acid digestions. Fresenius J. Anal. Chem. 359 (4–5), 468–472. http://dx.doi.org/10.1007/s002160050614.

Shumilovskikh, L.S., Marret, F., Fleitmann, D., Arz, H.W., Nowaczyk, N., Behling, H., 2013a. Eemian and Holocene sea-surface conditions in the southern Black Sea: Organic-walled dinoflagellate cyst record from core 22-GC3. Mar. Micropaleontol. 101, 146–160. http://dx.doi.org/10.1016/j.marmicro.2013.02.001.

Shumilovskikh, L.S., Arz, H.W., Wegwerth, A., Fleitmann, D., Marret, F., Nowaczyk, N., Tarasov, P., Behling, H., 2013b. Vegetation and environmental changes in Northern Anatolia between 134 and 119 ka recorded in Black Sea sediments. Quat. Res. 80, 349-360. http://dx.doi.org/10.1016/j.yqres.2013.07.005.

Shumilovskikh, L.S., Fleitmann, D., Nowaczyk, N.R., Behling, H., Marret, F., Wegwerth, A., Arz, H.W., 2014. Orbital- and millennial-scale environmental changes between 64 and 20 ka BP recorded in Black Sea sediments. Clim. Past. 10 (3), 939e954. http://dx.doi.org/10.5194/cp-10-939-2014.

Sima, A., Kageyama, M., Rousseau, D.D., Ramstein, G., Balkanski, Y., Antoine, P., Hatté, C., 2013. Modeling dust emission response to North Atlantic millennial-scale climate variations from the perspective of East European MIS 3 loess deposits. Clim. Past 9, 1385-1402. http://dx.doi.org/10.5194/cp-9-1385-2013.

Sinopoli, G., Masi, A., Regattieri, E., Wagner, B., Francke, A., Peyron, O., Sadori, L., 2018. Palynology of the Last Interglacial Complex at Lake Ohrid: palaeoenvironmental and palaeoclimatic inferences. Quaternary Science Reviews 180, 177-192. https://doi.org/10.1016/j.quascirev.2017.11.013

Smith, P.E., York, D., Chen, Y., Evensen, N.M., 1996. Single crystal 40Ar-39Ar dating of a Late Quaternary paroxysm on Kos, Greece: Concordance of terrestrial and marine ages. Geophys. Res. Lett. 23, 3047-3050. https://doi.org/10.1029/96GL02759.

Soulet, G., Ménot, G., Bayon, G., Rostek, F., Ponzevera, E., Toucanne, S., Lericolais, G., Bard, E., 2013. Abrupt drainage cycles of the Fennoscandian Ice Sheet. Proc. Nat. Acad. Sci. 110, 6682e6687. http://dx.doi.org/10.1073/pnas.1214676110.

Staneva, J.V., Stanev, E.V., 1998. Oceanic response to atmospheric forcing derived from different climatic data sets. Intercomparison study for the Black Sea. Ocean. Acta 21, 393e417. http://dx.doi.org/10.1016/S0399-1784(98)80026-1.

Stevens, L., Djamali, M., Andrieu-Ponel, V., de Beaulieu, J.-L., 2012. Hydroclimatic variations over the last two glacial/interglacial cycles at Lake Urmia, Iran. J. Paleolimnol. 47, 645-660. https://doi.org/10.1007.

Stockhecke, M., Timmermann, A., Kipfer, R., Haug, G.H., Kwiecien, O., Friedrich, T., Menviel, L., Litt, T., Pickarski, N., Anselmetti, F.S., 2016. Millennial to orbital-scale variations of drought intensity in the Eastern Mediterranean. Quat. Sci. Rev. 133, 77-95. https://doi.org/10.1016/j.quascirev.2015.12.016.

Svendsen, J.I., Alexanderson, H., Astakhov, V.I., Demidov, I., Dowdeswell, J.A., Funder, S., Gataullin, V., Henriksen, M., Hjort, C., Houmark-Nielsen, M., Hubberten, H.W., Ingólfsson, Ó., Jakobsson, M., Kjær, K.H., Larsen, E., Lokrantz, H., Lunkka, J.P., Lysså, A., Mangerud, J., Matiouchkov, A., Murray, A., Möller, P., Niessen, F., Nikolskaya, O., Polyak, L., Saarnisto, M., Siegert, C., Siegert, M.J., Spielhagen, R.F., Stein, R., 2004. Late Quaternary ice sheet history of northern Eurasia. Quat. Sci. Rev. 23, 1229-1271. https://doi.org/10.1016/j.quascirev.2003.12.008.

Svitoch, A.A., Selivanov, A.O., Yanina, T.A., 2000. Paleohydrology of the Black Sea Pleistocene Basins. Water Resources 27, 594-603. https://doi.org/10.1023/A:1026661801941.

Tomlinson, E.L., Kinvig, H.S., Smith, V.C., Blundy, J.D., Gottsmann, J., Müller, W. and Menzies, M. A. 2012. The Upper and Lower Nisyros Pumices: Revisions to the Mediterranean tephrostratigraphic record based on micron-beam glass geochemistry. J. Volcanol. Geoth. Res. 243-244, 69-80. https://doi.org/10.1016/j.jvolgeores.2012.07.004.

Tomlinson, E L., Smith, V.C., Albert, P.G., Aydar, E., Civetta, L., Cioni, R., Cubukcu, E., Gertisser, R., Isaia, R., Menzies, M. A., Orsi, G., Rosi, M. and Zanchetta, G. 2015. The major and trace element glass compositions of the productive Mediterranean volcanic sources: tools for correlating distal tephra layers in and around Europe. Quat. Sci. Rev. 118, 48-66. https://doi.org/10.1016/j.quascirev.2014.10.028

Toucanne, S., Zaragosi, S., Bourillet, J.F., Cremer, M., Eynaud, F., Van Vliet-Lanoë, B., Penaud, A., Fontanier, C., Turon, J.L., Cortijo, E., Gibbard, P.L., 2009. Timing of massive 'Fleuve Manche' discharges over the last 350 kyr: insights into the European ice-sheet oscillations and the European drainage network from MIS 10 to 2. Quat. Sci. Rev. 28, 1238-1256. https://doi.org/10.1016/j.quascirev.2009.01.006.

Türkeş, M., Koç, T., Sariş, F., 2009. Spatiotemporal variability of precipitation total series over Turkey. Int. J. Climatol. 29, 1056-1074. http://dx.doi.org/10.1002/joc.1768.

Tryon, C.A., Logan, M.A.V., Mouralis, D., Kuhn, S., Slimak, L. and Balkan-Atli, N. 2009. Building a tephrostratigraphic framework for the Paleolithic of Central Anatolia, Turkey. J. Archaeol. Sci. 36, 637-652. https://doi.org/10.1016/j.jas.2008.10.006.

Van Baak, C.G.C., Grothe, A., Richards, K., Stoica, M., Aliyeva, E., Davies, G.R., Kuiper, K.F., Krijgsman, W., 2019. Flooding of the Caspian Sea at the intensification of Northern Hemisphere Glaciations. Glob. Planetary Change 174, 153-163. https://doi.org/10.1016/j.gloplacha.2019.01.007

van Hardenbroek, M., Chakraborty, A., Davies, K.L., Harding, P., Heiri, O., Henderson, A.C.G., Holmes, J.A., Lasher, G.E., Leng, M.J., Panizzo, V.N., Roberts, L., Schilder, J., Trueman, C.N., Wooller, M.J., 2018. The stable isotope composition of organic and inorganic fossils in lake sediment records: Current understanding, challenges, and future directions. Quat. Sci. Rev. 196, 154-176. https://doi.org/10.1016/j.quascirev.2018.08.003.

Vasiliev, I., Reichart, G.-J., Davies, G.R., Krijgsman, W., Stoica, M., 2010. Strontium isotope ratios of the Eastern Paratethys during the Mio-Pliocene transition; Implications for interbasinal connectivity. Earth Planet. Sci. Lett. 292, 123-131. https://doi.org/10.1016/j.epsl.2010.01.027.

Vinci, A. 1985. Distribution and chemical composition of tephra layers from Eastern Mediterranean abyssal sediments. Mar. Geol. 64, 143-155. https://doi.org/10.1016/0025-3227(85)90165-3.

Vogel, H., Wagner, B., Zanchetta, G., Sulpizio, R., Rosén, P., 2010. A paleoclimate record with tephrochronological age control for the last glacial-interglacial cycle from Lake Ohrid, Albania and Macedonia. J. Paleolimnol. 44, 295-310. https://doi.org/10.1007/s10933-009-9404-x.palaeog

von Grafenstein, U., Erlernkeuser, H., Trimborn, P., 1999. Oxygen and carbon isotopes in modern fresh-water ostracod valves: assessing vital offsets and autecological effects of interest for palaeoclimate studies. Palaeogeogr. Palaeoclimatol. Palaeoecol. 148, 133-152. https://doi.org/10.1016/S0031-0182(98)00180-1.

Wainer, K., Genty, D., Blamart, D., Bar-Matthews, M., Quinif, Y., Plagnes, V., 2013. Millennial climatic instability during penultimate glacial period recorded in a south-western France

speleothem. Palaeogeogr. Palaeoclimatol. Palaeoecol. 376, 122-131. https://doi.org/10.1016/j.palaeo.2013.02.026

Wang, Y., Cheng, H., Edwards, R.L., Kong, X., Shao, X., Chen, S., Wu, J., Jiang, X., Wang, X., An, Z., 2008. Millennial- and orbital-scale changes in the East Asian monsoon over the past 224,000 years. Nature 451, 1090-1093. https://doi.org/10.1038/nature06692.

Wansard, G., De Deckker, P., Julià, R., 1998. Variability in ostracod partition coefficients D(Sr) and D(Mg) : Implications for lacustrine palaeoenvironmental reconstructions. Chem. Geol. 146, 39-54. https://doi.org/10.1016/S0009-2541(97)00165-4

Wegwerth, A., Dellwig, O., Kaiser, J., Ménot, G., Bard, E., Shumilovskikh, L., Schnetger, B., Kleinhanns, I.C., Wille, M., Arz, H.W., 2014. Meltwater events and the Mediterranean reconnection at the Saalian–Eemian transition in the Black Sea. Earth Planet. Sci. Lett. 404, 124-135. https://doi.org/10.1016/j.epsl.2014.07.030.

Wegwerth, A., Ganopolski, A., Ménot, G., Kaiser, J., Dellwig, O., Bard, E., Lamy, F., Arz, H.W., 2015. Black Sea temperature response to glacial millennial-scale climate variability. Geophys. Res. Lett. 42, 2015GL065499. https://doi.org/10.1002/2015GL065499.

Wegwerth, A., Kaiser, J., Dellwig, O., Shumilovskikh, L.S., Nowaczyk, N.R., Arz, H.W., 2016. Northern hemisphere climate control on the environmental dynamics in the glacial Black Sea "Lake". Quat. Sci. Rev. 135, 41-53. https://doi.org/10.1016/j.quascirev.2016.01.016

Wegwerth, A., Eckert, S., Dellwig, O., Schnetger, B., Severmann, S., Weyer, S., Brüske, A., Kaiser, J., Köster, J., Arz, H.W., Brumsack, H.-J., 2018. Redox evolution during Eemian and Holocene sapropel formation in the Black Sea. Palaeogeogr. Palaeoclimatol. Palaeoecol. 489, 249-260. https://doi.org/10.1016/j.palaeo.2017.10.014.

Widerlund, A., Andersson, P.S., 2006. Strontium isotopic composition of modern and Holocene mollusc shells as a palaeosalinity indicator for the Baltic Sea. Chem. Geol. 232, 54-66. https://doi.org/10.1016/j.chemgeo.2006.02.010.

Wigley, T.M.L., Farmer, G., (1982). Climate of the Eastern Mediterranean and Near East. In: Palaeoclimates, Palaeoenvironments and Human Communities in the Eastern Mediterranean Region of Later Prehistory (Eds. J.L. Bintliff and W. van Zeist), pp.3-39 B.A.R. International Series 133(i).

Wulf, S., Hardiman, M.J., Staff, R.A., Koutsodendris, A., Appelt, O., Blockley, S.P.E., Lowe, J.J., Manning, C.J., Ottolini, L., Schmitt, A.K., Smith, V.C., Tomlinson, E.L., Vakhrameeva, P., Knipping, M., Kotthoff, U., Milner, A.M., Müller, U.C., Christanis, K., Kalaitzidis, S., Tzedakis, P.C., Schmiedl, G., Pross, J., 2018. The marine isotope stage 1–5 cryptotephra record of Tenaghi Philippon, Greece: Towards a detailed tephrostratigraphic framework for the Eastern Mediterranean region. Quat. Sci. Rev. 186, 236-262. https://doi.org/10.1016/j.quascirev.2018.03.011.

Wulf, S., Keller, J.r., Paterne, M., Mingram, J., Lauterbach, S., Opitz, S., Sottili, G., Giaccio, B., Albert, P.G., Satow, C., Tomlinson, E.L., Viccaro, M., Brauer, A., 2012. The 100-133 ka record of Italian explosive volcanism and revised tephrochronology of Lago Grande di Monticchio. Quat. Sci. Rev. 58, 104-123. https://doi.org/10.1016/j.quascirev.2012.10.020.

Yanchilina, A.G., Ryan, W.B.F., McManus, J.F., Dimitrov, P., Dimitrov, D., Slavova, K., Filipova-Marinova, M., 2017. Compilation of geophysical, geochronological, and geochemical evidence indicates a rapid Mediterranean-derived submergence of the Black Sea's shelf and subsequent substantial salinification in the early Holocene. Mar. Geol. 383, 14-34. https://doi.org/10.1016/j.margeo.2016.11.001.

Zubakov, V.A., 1988. Climatostratigraphic scheme of the Black Sea pleistocene and its correlation with the oxygen-isotope scale and glacial events. Quat. Res. 29, 1-24. https://doi.org/10.1016/0033-5894(88)90067-1

Figure captions

Fig. 1. Map showing Eurasia including the coring site of MSM 33 in the Black Sea (yellow star), regions discussed in the text and the maximum extent of the Eurasian Ice Sheet during the Saalian (MIS 6; modified from Svendsen et al., 2004) and Weichselian (MIS 2 and 3; modified from Larsen et al., 2006). The 100 m isobath in the Black Sea gives an idea about the glacial Black Sea "Lake" level. Arrows indicate potential meltwater pathways during different periods of MIS 6; 'Fleuve Manche' discharge adapted from Toucanne et al. (2009). BSWP refer to Black Sea water pulses. BS=Black Sea, MD=Manych Depression, CS=Caspian Sea, AS=Aral Sea, MS=Marmara Sea, AeS=Aegean Sea, SC=Sofular Cave, AC=Abaliget Cave; rivers: S= Sakarya, K=Kizilirmak, Y=Yesilirmak. The inlay shows a detailed map of the study area with core locations at the Archangelsky Ridge; gravity cores: 1) M72/5/22GC-8, 2) MSM33/61-1GC, 3) MSM33/60-1GC, 4) MSM33/57-1GC and MSM33/56-1GC.

Fig. 2: Ca/Ti_{XRF} ratios of cores MSM33/60-1GC, MSM33/57-1GC and MSM33/56-1GC and the composite core profile.

Fig. 3: Bivariate elemental plots of tephra glass chemical data for tephra source identification. Data used for comparison are from Federman and Carey (1980), Vinci (1985), Tryon et al. (2009), Schmincke and Sumita (2014), Bourne et al. (2015), Tomlinson et al. (2012, 2015), Satow et al. (2015), Leicher et al. (2016), and Giaccio et al. (2017). Lago Grande di Monticchio (TM) tephra data derived from Wulf et al. (2012).

Fig. 4. Age-depth relation of composite core from MSM33 expedition constructed by correlation of the $\delta^{18}O_{ostracod}$ record of the composite core with $\delta^{18}O$ records of speleothems from Sofular Cave (Anatolia; Badertscher et al., 2011) and Abaliget Cave (Hungary; Koltai et al., 2017). Further age control points come from the tephra analyses. The unknown tephra forms a time marker adapted from a dated parallel core (M72/5/22GC-8; Wegwerth et al., 2014). The inlay shows the correlation of tie points between the composite core and core M72/5/22GC-8 with an already existing age model (Shumilovskikh et al., 2013a, b; Wegwerth et al., 2014) for the youngest part of the record.

Fig. 5. Temporal variation of environmental proxies of the composite core during MIS 6 and the onset of MIS 5e (184-124 ka BP). A) $\delta^{18}O$ of the ostracods; B) Mg/Ca ratios of the ostracods; C) Sr/Ca ratios of the ostracods; D) $^{87}Sr/^{86}Sr$ record of the ostracods of the present composite core (filled circles) and core M72/5/22GC-8 (white circles; Wegwerth et al., 2014); E) number of coastal ice-rafted detritus (IRD_C); F) content of total inorganic carbon (TIC); G) content of total organic carbon (TOC); H) $ln(K/Ti)_{XRF}$. The thick lines in B, C, and E show the simple 3-point moving average. The vertical dashed line indicates the Mediterranean-Black Sea reconnection and triangles position of the tephra samples. MIS 6 substages a-e were adapted from Railsback et al. (2015).

Fig. 6. Temporal variation of A) summer insolation at 65°N (Berger and Loutre, 1991); B) smoothed relative sea level (Grant et al., 2012); C) Eurasian Ice Sheet (EIS) volume relative to present (Bintanja and van de Wal, 2008); D) $\delta^{18}O$ variations of a synthetic Greenland ice core reflecting temperature changes (Barker et al., 2011); E) alkenone-based sea surface temperatures (SST) in the western Mediterranean Sea (Martrat et al., 2004); F) Mg/Ca ratios of the ostracods (this study); G) $\delta^{18}O$ record of Sofular speleothems So-6-3 and So-4 (Badertscher et al., 2011); H) $\delta^{18}O$ of the ostracods (this study); I) $^{87}Sr/^{86}Sr$ record of the ostracods of the present composite core (filled circles) and core M72/5/22GC-8 (white circles, Wegwerth et al., 2014) dashed line indicates the modern $^{87}Sr/^{86}Sr$ level in the Black Sea (Major et al., 2006). Vertical grey bars denote meltwater periods. BSWP refer to Black Sea water pulses. MIS 6 substages a-e were adapted from Railsback et al. (2015).

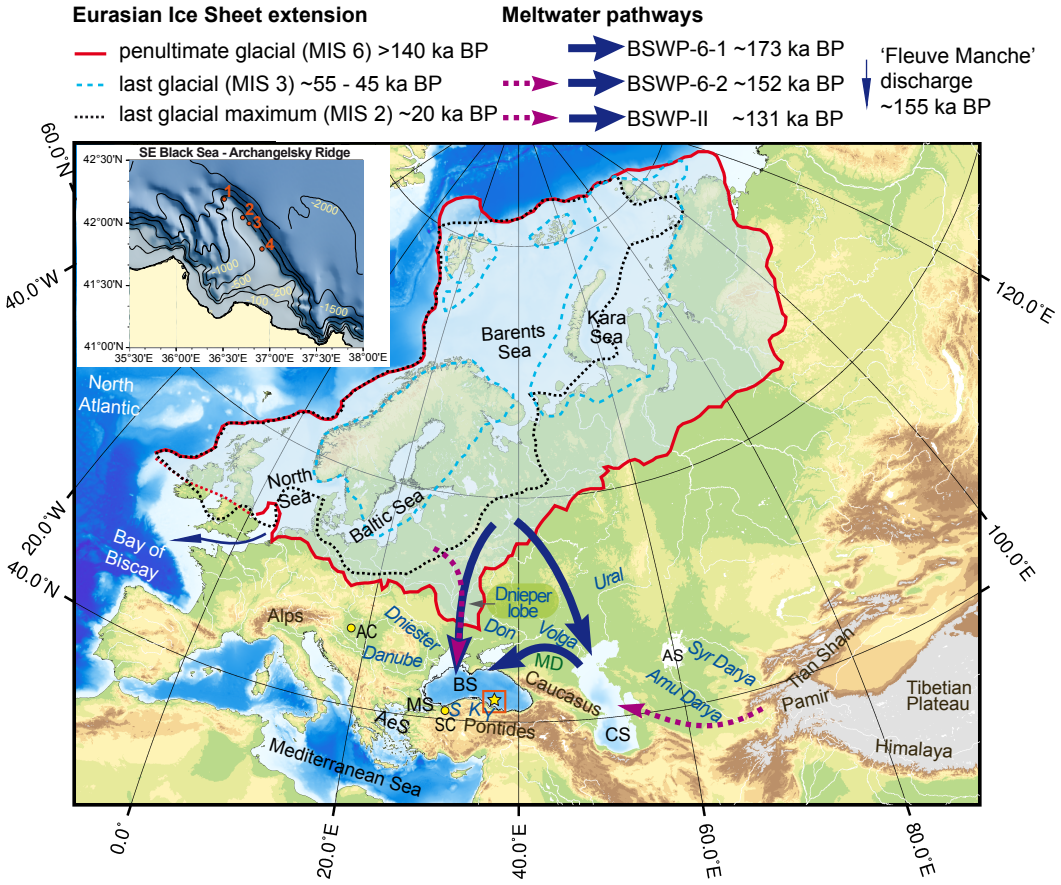
Eurasian Ice Sheet extension
penultimate glacial (MIS 6) >140 ka BP
last glacial (MIS 3) ~55 - 45 ka BP
last glacial maximum (MIS 2) ~20 ka BP
Meltwater pathways
BSWP-6-1 ~173 ka BP
BSWP-6-2 ~152 ka BP
BSWP-II ~131 ka BP
'Fleuve Manche' discharge ~155 ka BP
SE Black Sea - Archangelsky Ridge
42°30'N
42°00'N
41°30'N
41°00'N
35°30'E
36°00'E
36°30'E
37°00'E
37°30'E
38°00'E
2000
1500
Barents Sea
Kara Sea
North Atlantic
North Sea
Baltic Sea
Bay of Biscay
Alps
AC
Dniester
Danube
Dnieper lobe
Don
Volga
Ural
MD
Caucasus
BS
MS
S K
SC
Pontides
AeS
CS
AS
Syr Darya
Amu Darya
Tian Shan
Pamir
Tibetan Plateau
Himalaya
Mediterranean Sea
60.0°N
40.0°W
20.0°W
40.0°N
120.0°E
100.0°E
0.0°
20.0°E
40.0°E
60.0°E
80.0°E

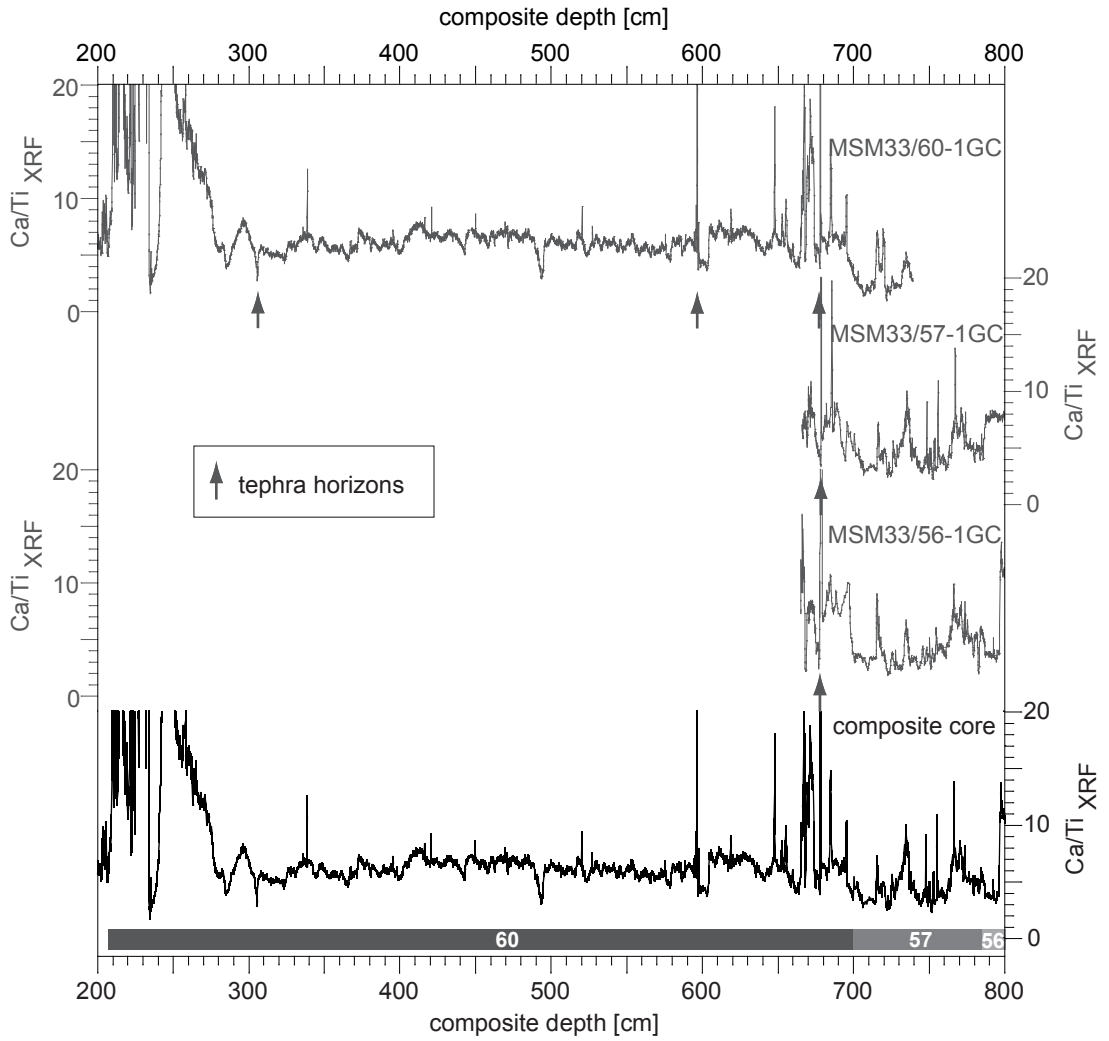
composite depth [cm]
200
300
400
500
600
700
800
Ca/Ti XRF
20
10
0
MSM33/60-1GC
MSM33/57-1GC
MSM33/56-1GC
tephra horizons
composite core
60
57
56
composite depth [cm]

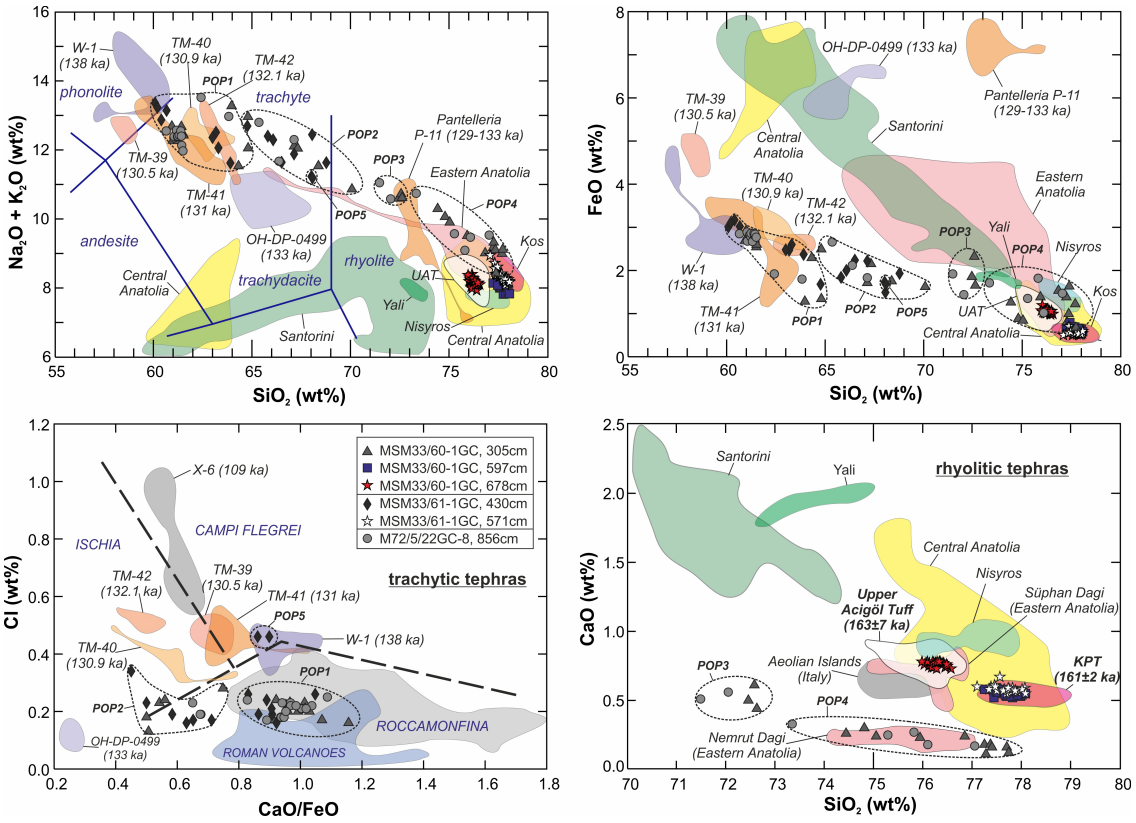
W-1 (138 ka)
TM-40 (130.9 ka)
TM-42 (132.1 ka)
POP1
phonolite
trachyte
POP2
POP3
Pantelleria P-11 (129-133 ka)
Eastern Anatolia
TM-39 (130.5 ka)
TM-41 (131 ka)
POP4
POP5
andesite
OH-DP-0499 (133 ka)
Kos
rhyolite
Central Anatolia
trachydacite
UAT
Yali
Nisyros
Santorini
Central Anatolia
Na2O + K2O (wt%)
SiO2 (wt%)
OH-DP-0499 (133 ka)
Pantelleria P-11 (129-133 ka)
Santorini
TM-39 (130.5 ka)
Central Anatolia
Eastern Anatolia
TM-40 (130.9 ka)
TM-42 (132.1 ka)
POP3
Yali
POP4
Nisyros
W-1 (138 ka)
Kos
TM-41 (131 ka)
POP1
POP2
POP5
UAT
Central Anatolia
FeO (wt%)
SiO2 (wt%)
MSM33/60-1GC, 305cm
MSM33/60-1GC, 597cm
MSM33/60-1GC, 678cm
MSM33/61-1GC, 430cm
MSM33/61-1GC, 571cm
M72/5/22GC-8, 856cm
X-6 (109 ka)
CAMPI FLEGREI
ISCHIA
TM-42 (132.1 ka)
TM-39 (130.5 ka)
TM-41 (131 ka)
trachytic tephras
POP5
W-1 (138 ka)
TM-40 (130.9 ka)
POP1
POP2
ROCCAMONFINA
OH-DP-0499 (133 ka)
ROMAN VOLCANOES
Cl (wt%)
CaO/FeO
Santorini
Yali
rhyolitic tephras
Central Anatolia
Nisyros
Upper Acigöl Tuff (163±7 ka)
Süphan Dagi (Eastern Anatolia)
POP3
Aeolian Islands (Italy)
KPT (161±2 ka)
POP4
Nemrut Dagi (Eastern Anatolia)
CaO (wt%)
SiO2 (wt%)

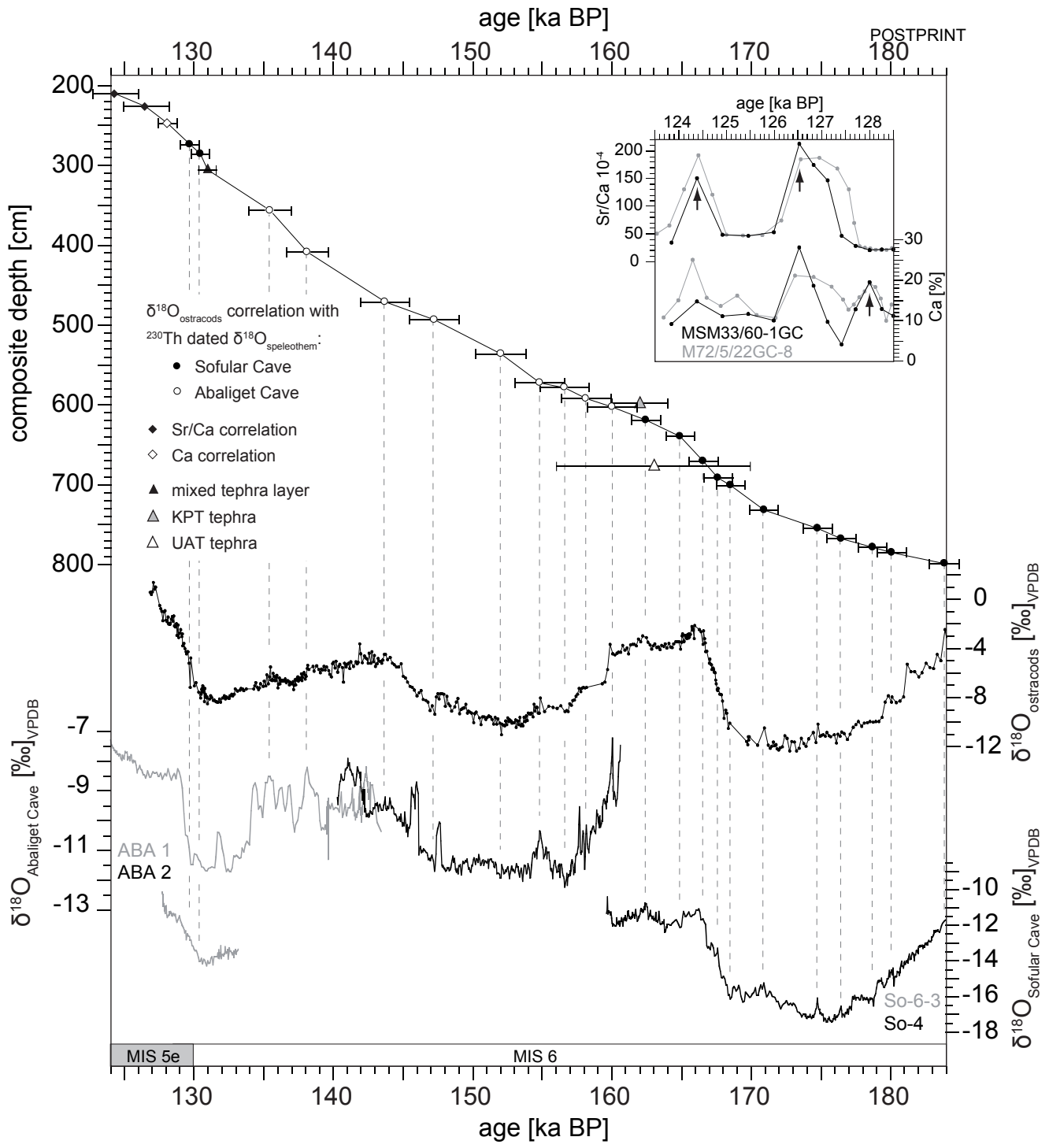
age [ka BP]
composite depth [cm]
δ18Oostracods correlation with
230Th dated δ18Ospeleothem:
Sofular Cave
Abaliget Cave
Sr/Ca correlation
Ca correlation
mixed tephra layer
KPT tephra
UAT tephra
Sr/Ca 10-4
Ca [%]
MSM33/60-1GC
M72/5/22GC-8
δ18Oostracods [‰]VPDB
δ18OAbaliget Cave [‰]VPDB
δ18OSofular Cave [‰]VPDB
ABA 1
ABA 2
So-6-3
So-4
MIS 5e
MIS 6

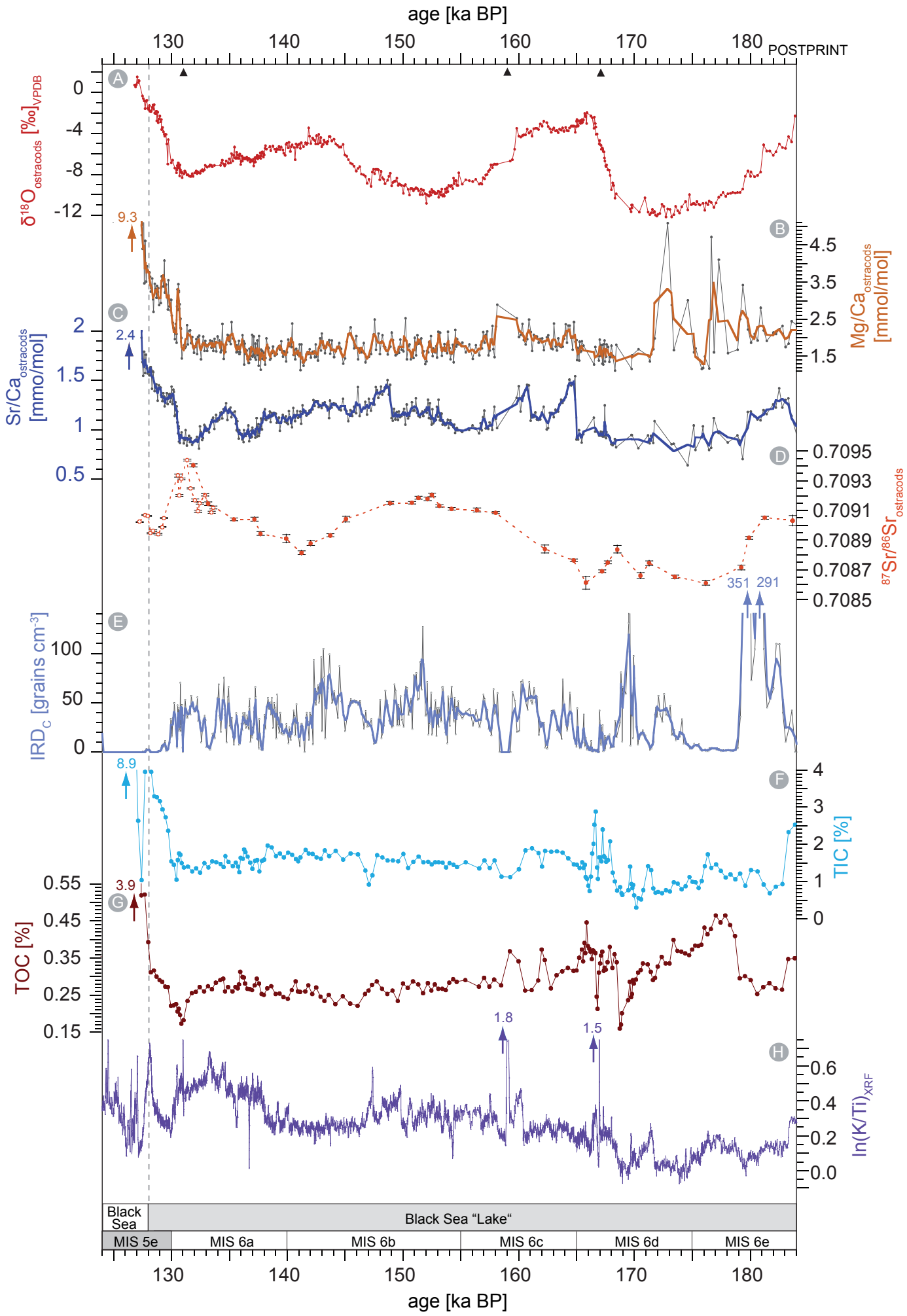
age [ka BP]
130
140
150
160
170
180
POSTPRINT
A
$\delta^{18}O_{ostracods}$ [‰]$_{VPDB}$
0
-4
-8
-12
9.3
B
Mg/Ca$_{ostracods}$ [mmol/mol]
4.5
3.5
2.5
1.5
C
Sr/Ca$_{ostracods}$ [mmo/mol]
2
1.5
1
0.5
2.4
D
$^{87}Sr/^{86}Sr_{ostracods}$
0.7095
0.7093
0.7091
0.7089
0.7087
0.7085
351
291
E
IRD$_C$ [grains cm^{-3}]
100
50
0
F
TIC [%]
4
3
2
1
0
8.9
G
TOC [%]
0.55
0.45
0.35
0.25
0.15
3.9
H
ln(K/Ti)$_{XRF}$
0.6
0.4
0.2
0.0
1.8
1.5
Black Sea
Black Sea "Lake"
MIS 5e
MIS 6a
MIS 6b
MIS 6c
MIS 6d
MIS 6e
130
140
150
160
170
180
age [ka BP]

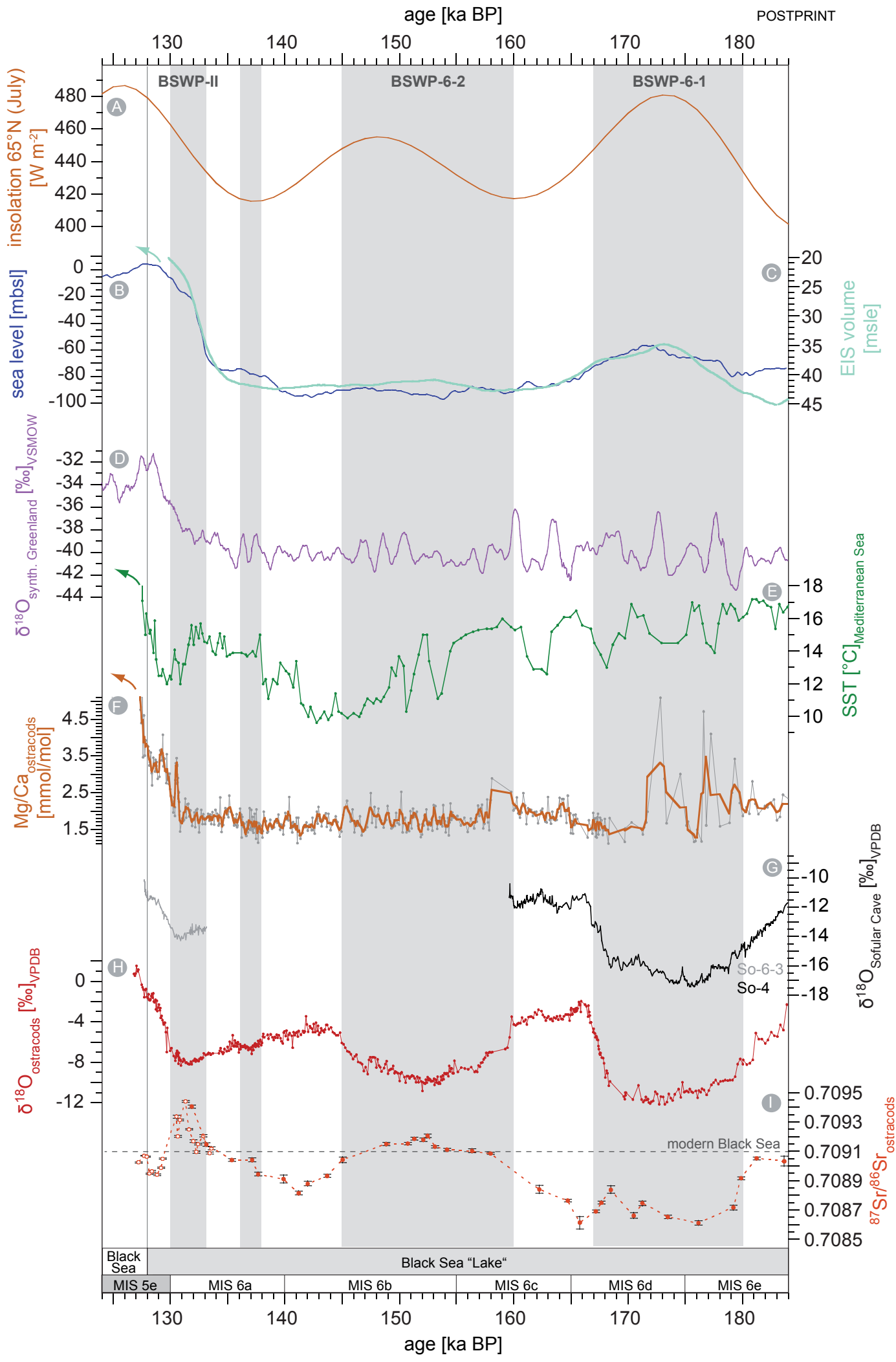
age [ka BP]
130
140
150
160
170
180
BSWP-II
BSWP-6-2
BSWP-6-1
A
insolation 65°N (July) [W m-2]
480
460
440
420
400
B
sea level [mbsl]
0
-20
-40
-60
-80
-100
C
EIS volume [msle]
20
25
30
35
40
45
D
δ18Osynth. Greenland [‰]VSMOW
-32
-34
-36
-38
-40
-42
-44
E
SST [°C]Mediterranean Sea
18
16
14
12
10
F
Mg/Caostracods [mmol/mol]
4.5
3.5
2.5
1.5
G
δ18OSofular Cave [‰]VPDB
-10
-12
-14
-16
-18
So-6-3
So-4
H
δ18Oostracods [‰]VPDB
0
-4
-8
-12
I
87Sr/86Srostracods
0.7095
0.7093
0.7091
0.7089
0.7087
0.7085
modern Black Sea
Black Sea
Black Sea "Lake"
MIS 5e
MIS 6a
MIS 6b
MIS 6c
MIS 6d
MIS 6e
age [ka BP]

Table 1: $^{87}Sr/^{86}Sr$ data for different water sources and (pre-)Holocene carbonate shells; BSWP=Black Sea Water Pulse; T I/T II=Termination I/II.

material	$^{87}Sr/^{86}Sr$	reference
water		
modern ocean water	0.709155 – 0.709172	Henderson et al., 1994; Meknassi et al., 2018
Black Sea	0.7093	Cox and Faure, 1974
	0.709133	Major et al., 2006
	0.709120 – 0.709155	Ankindinova et al., 2019
Caspian Sea	0.70821 – 0.7085	Clauer et al. 2000; Palmer and Edmond, 1989; Page et al., 2003
Aegean Sea	0.709157	Major et al., 2006
Marmara Sea	0.709150	Major et al., 2006
Danube	0.7089	Palmer and Edmond,1989
Dnieper	0.7084	Palmer and Edmond,1989
Don	0.7084	Palmer and Edmond,1989
Sakarya	0.7089	Major et al., 2006
Volga	0.70802 – 0.708083	Clauer et al., 2000; Page et al., 2003
Ural	0.7082	Vasiliev et al., 2010
Syr Darya / av. Aral Sea	0.70940 / 0.70914	Pokrovsky et al., 2017
Lesser Himalayan streams	0.7166 – 1.023	Jacobson et al., 2002
ostracods/molluscs		
Black Sea BSWP T I	0.708808 – 0.709102	Major et al., 2006
Black Sea BSWP T II	0.709092 – 0.709452	Wegwerth et al., 2014; this study
Black Sea BSWP-6-2	0.709044 – 0.709207	this study
Black Sea BSWP-6-1	0.708612 – 0.709033	this study
Paratethys (Mio-/Pliocene)	0.70865 – 0.70885	Vasiliev et al., 2010
Caspian Sea at 100 ka BP max.	0.70842 – 0.70864	Page et al., 2003
Baltic Sea (modern)	0.709566	Widerlund and Andersson, 2006
Baltic Sea (subfossil, Holocene)	0.709306	Widerlund and Andersson, 2006